Published in final edited form as:

Nat Immunol. 2020 January ; 21(1): 54–64. doi:10.1038/s41590-019-0550-7.

Ptpn6 inhibits caspase-8- and Ripk3/Mlkl-dependent inflammation

Mary Speir[1,2,3,4], **Cameron J. Nowell**[5], **Alyce A. Chen**[1,2], **Joanne A. O'Donnell**[6,7], **Isaac S. Shamie**[8], **Paul R. Lakin**[9], **Akshay A. D'Cruz**[1,2], **Roman O. Braun**[1,2], **Jeff J. Babon**[6,7], **Rowena S. Lewis**[6,7], **Meghan Bliss-Moreau**[1,2], **Inbar Shlomovitz**[10], **Shu Wang**[1,2], **Louise H. Cengia**[6], **Anca I. Stoica**[1], **Razq Hakem**[11], **Michelle A. Kelliher**[12], **Lorraine A. O'Reilly**[6,7], **Heather Patsiouras**[13], **Kate E Lawlor**[3,4], **Edie Weller**[1,9], **Nathan E. Lewis**[8,14,15], **Andrew W. Roberts**[6,7], **Motti Gerlic**[10], **Ben A. Croker**[*,1,2,6,7,8]

[1.]Division of Hematology/Oncology, Boston Children's Hospital, Boston, Massachusetts, USA

[2.]Department of Pediatrics, Harvard Medical School, Boston Massachusetts, USA

[3.]Centre for Innate Immunity and Infectious Diseases, Hudson Institute of Medical Research, Clayton, Victoria, 3168, Australia

[4.]Department of Molecular and Translational Science, Monash University, Clayton, Victoria, 3168, Australia

[5.]Monash Institute of Pharmaceutical Sciences, Parkville, Victoria 3052, Australia

[6.]Walter and Eliza Hall Institute of Medical Research, Parkville, Victoria 3052, Australia

[7.]Department of Medical Biology, University of Melbourne, Parkville, Victoria 3010, Australia

[8.]Department of Pediatrics, University of California San Diego, La Jolla, California, USA

[9.]Biostatistics and Research Design Center, Institutional Centers for Clinical and Translational Research, Boston Children's Hospital, Boston, Massachusetts, USA

[10.]Department of Clinical Microbiology and Immunology, Sackler Faculty of Medicine, Tel Aviv University, Tel Aviv 69978, Israel

[11.]University of Toronto, Princess Margaret Cancer Centre/University Health Network, Toronto, Canada

[*]Correspondence: Ben Croker, Department of Pediatrics, School of Medicine, UC San Diego, 9500 Gilman Drive MC 0760, La Jolla, CA 92093-0760. bcroker@health.ucsd.edu.

Author Contributions

Project design: MS, AAC, JAO, AAD, JJB, RSL, MBM, IS, KEL, AIS, AWR, MG, BAC
Analysis: MS, CJN, AAC, JAO, ISS, PRL, AAD, ROB, JJB, RSL, MBM, IS, SW, LHC, AIS, HP, KEL, EW, NEL, AWR, MG, BAC
Funding: AWR, EW, NEL, KEL, RH, MAK, JJB, CJN, BAC
Experiments: MS, AAC, JAO, AAD, ROB, JJB, RSL, MBM, IS, SW, LHC, AIS, HP, LAO, KEL, MG, BAC
Software development: CJN
Supervision: MS, AAC, JJB, EW, NEL, KEL, AWR, MG, BAC
Writing: MS, JAO, KEL, NEL, IS, MG, BAC

Disclosure of Conflicts of Interest

The authors declare no competing financial or non-financial conflicts of interest.

[12.]Department of Molecular, Cell and Cancer Biology, University of Massachusetts Medical School, Worcester, Massachusetts, USA

[13.]Ludwig Institute for Cancer Research, Royal Melbourne Hospital, Melbourne, Victoria 3052, Australia

[14.]Department of Bioengineering, University of California San Diego, La Jolla, California, USA

[15.]Novo Nordisk Foundation Center for Biosustainability, University of California San Diego, La Jolla, California, USA

Abstract

Ptpn6 is a cytoplasmic phosphatase that functions to prevent autoimmune and interleukin 1 receptor (IL-1R)-dependent caspase-1-independent inflammatory disease. Conditional deletion of *Ptpn6* in neutrophils (*Ptpn6*$^{\Delta PMN}$) is sufficient to initiate IL-1R-dependent cutaneous inflammatory disease, but the source of IL-1 and the mechanisms behind IL-1 release remain unclear. Here, we investigated the mechanisms controlling IL-1α/β release from neutrophils by inhibiting caspase-8-dependent apoptosis and Ripk1–Ripk3–Mlkl-regulated necroptosis. Loss of Ripk1 accelerated disease onset, whereas combined deletion of caspase-8, and either Ripk3 or Mlkl, strongly protected *Ptpn6*$^{\Delta PMN}$ mice. *Ptpn6*$^{\Delta PMN}$ neutrophils displayed increased p38 MAP kinase-dependent Ripk1-independent IL-1 and tumor necrosis factor (TNF) production, and were prone to cell death. Together, these data emphasize dual functions for Ptpn6 in the negative regulation of p38 MAP kinase activation to control TNF and IL-1α/β expression, and in maintaining Ripk1 function to prevent caspase-8- and Ripk3–Mlkl-dependent cell death and concomitant IL-1α/β release.

Keywords

Ptpn6; Shp1; Ripk1; caspase-8; Ripk3; Mlkl; neutrophil; necroptosis; cell death; apoptosis

INTRODUCTION

Neutrophilic dermatoses are a group of inflammatory skin disorders characterized by sterile infiltrates of neutrophils. These syndromes include pyoderma gangrenosum (PG) and Sweet's syndrome (SS), and are associated with an increased risk of inflammatory bowel disease, rheumatoid arthritis, and hematologic malignancy, particularly chronic myelogenous and acute myeloid leukemia.[1–3] Interleukin-1 (IL-1) has been reported at high concentrations in the lesions of SS patients, and IL-1 neutralizing therapies have shown promising outcomes in SS, PG, and PG patients with psoriatic arthritis.[4–9] Coding and transcript variants of protein tyrosine phosphatase-6 (PTPN6, or Src homology region 2 domain-containing phosphatase-1, SHP1) are a feature of SS and PG, consistent with the findings that mutations in murine *Ptpn6* cause spontaneous skin inflammation that is dependent on the IL-1 receptor (IL-1R), granulocyte-colony stimulating factor (G-CSF), and neutrophils.[10–13]

Ptpn6 regulates the activity of more than 50 cytoplasmic signaling proteins and cell surface receptors. In its absence, *motheaten* (*Ptpn6*$^{me/me}$) and *motheaten viable* (*Ptpn6*$^{mev/mev}$)

Ptpn6 mutant mice succumb to IL-1R- and macrophage-dependent lethal pneumonitis at three and 10 weeks-of-age, respectively.[14,15] In contrast, mice with the Y208N mutation (*Ptpn6*$^{Y208N/Y208N}$) develop a neutrophilic, IL-1R- and G-CSF-dependent cutaneous inflammatory disease without pneumonitis.[11] Gnotobiotic *Ptpn6*$^{Y208N/Y208N}$ mice do not develop inflammation of the skin, indicating that this is not an autoinflammatory disease.[11] TNF is not essential for disease induction but TNF neutralizing antibodies ameliorate the IL-1R-dependent pulmonary fibrosis observed in *Ptpn6* mutant mice, and TNF-deficiency reduces the incidence and delays the onset of disease in *Ptpn6*$^{Y208N/Y208N}$ mice.[15–17]

Perturbations in Toll-like receptor (TLR) signaling and cell death have been proposed to contribute to inflammatory disease driven by IL-1α and IL-1β in *Ptpn6*$^{Y208N/Y208N}$ mice independently of caspase-1.[12] However, the precise caspase-1-independent pathway controlling IL-1 release from Ptpn6-deficient neutrophils remains undefined. Caspase-1-independent regulators of IL-1α and IL-1β processing and release include caspase-8 and the necroptotic effector proteins receptor-interacting protein kinase 1 (Ripk1), Ripk3, and mixed lineage kinase domain-like pseudokinase (Mlkl).[18–21] Here we examine the role of caspase-8 and Ripk3/Mlkl cell death signaling in regulating the release of IL-1α and IL-1β to drive pathological inflammation in Ptpn6 mutant mice.

RESULTS

Ptpn6 controls necroptosis in neutrophils

Both IL-1α and IL-1β lack signal peptides for secretion and, therefore, require alternative mechanisms of release, most notably via the actions of caspase-1/11. Previous studies in *Ptpn6*$^{Y208N/Y208N}$ mice have demonstrated that inflammasome-mediated caspase-1/11 activation is not involved in the IL-1-driven inflammation in this model.[11,12] Increasingly, other modes of IL-1 secretion are now being recognized in macrophages and neutrophils, including cell death signaling pathways associated with caspase-8-mediated apoptosis and Ripk3-Mlkl-mediated necroptosis.[18–21] To test the involvement of these cell death pathways in neutrophil-driven inflammation when Ptpn6 is absent, we generated mice deficient in *Ptpn6*, in combination with gene deficiency in *Casp8*, *Ripk1*, *Ripk3,* or *Mlkl*. We restricted deletion of the conditional *Ptpn6* allele to neutrophils to avoid lethal pneumonitis and autoimmune disease associated with germline *Ptpn6*-deficiency using the *S100a8-Cre* transgene (denoted ΔPMN). A conditional allele of *Ripk1* was utilized to avoid the perinatal lethality associated with germline Ripk1 deficiency.[19,22,23] To avoid potential *in vivo* artifacts caused by the Ripk1-regulated lymphoproliferative disease that develops in germline *Casp8*$^{-/-}$*Ripk3*$^{-/-}$ mice, *Casp8* deletion was similarly restricted.[19,22,24,25]

Previous studies have demonstrated that granulocyte colony-stimulating factor (G-CSF) does not protect *Ptpn6*$^{Y208N/Y208N}$ neutrophils from accelerated apoptotic cell death.[12] To investigate whether Ptpn6-deficient neutrophils were also sensitized to Ripk1-Ripk3-Mlkl necroptotic signaling, we cultured neutrophils with a combination of birinapant, a SMAC mimetic that targets the cellular inhibitor of apoptosis proteins, cIAP1 and cIAP2, for degradation and induces formation of an apoptotic death complex, and z-VAD-fmk, a pan-caspase inhibitor that blocks caspase-8 activity and converts the complex to a necroptotic cell death program. As expected, when neutrophils were treated with G-CSF or interferon-γ

(IFN-γ), increased cell death of *Ptpn6*$^{\Delta PMN}$ neutrophils was evident compared to wild-type and *Ptpn6*$^{\Delta PMN}$*Casp8*$^{\Delta PMN}$*Mlkl*$^{-/-}$ neutrophils (Fig. 1a,b). Analysis of necroptosis signaling in neutrophils using birinapant/z-VAD-fmk also revealed increased necroptotic cell death of *Ptpn6*$^{\Delta PMN}$ neutrophils compared to wild-type, while *Ptpn6*$^{\Delta PMN}$*Casp8*$^{\Delta PMN}$*Mlkl*$^{-/-}$ neutrophils were protected from this sensitization (Figure 1a,b). These data suggest that Ptpn6 functions in neutrophils to limit apoptotic and necroptotic cell death signaling.

Neutrophil death drives cutaneous inflammation

To examine whether apoptotic signaling is contributing to inflammation in *Ptpn6*$^{\Delta PMN}$ mice, we first examined caspase-8 activity in freshly-isolated bone marrow neutrophils. Cleaved caspase-8 was detected in unstimulated *Ptpn6*$^{\Delta PMN}$ neutrophils but not in neutrophils isolated from wild-type littermate controls (Fig. 2a). To test the absolute requirement for caspase-8-dependent apoptosis versus Ripk3-Mlkl-dependent necroptosis in the development of spontaneous neutrophil-driven footpad inflammation in *Ptpn6*$^{\Delta PMN}$ mice, we tracked the incidence of disease in *Ptpn6*$^{\Delta PMN}$*Casp8*$^{\Delta PMN}$*Ripk3*$^{-/-}$, *Ptpn6*$^{\Delta PMN}$*Casp8*$^{\Delta PMN}$*Mlkl*$^{-/-}$, and *Ptpn6*$^{\Delta PMN}$*Casp8*$^{\Delta PMN}$*Ripk3*$^{-/-}$*Mlkl*$^{-/-}$ mice (Fig. 2b). Importantly, *Ptpn6*$^{\Delta PMN}$ mice developed cutaneous footpad inflammation at the same rate as *Ptpn6*$^{Y208N/Y208N}$ mice, and as observed in other studies using *Ptpn6*$^{\Delta PMN}$ mice.[11–13,16] These data were also consistent with a previous report demonstrating that Ptpn6 deficiency in neutrophils is sufficient to trigger cutaneous inflammation.[13] Individual loss of necroptotic cell death signaling by deletion of *Ripk3* (*Ptpn6*$^{\Delta PMN}$*Ripk3*$^{-/-}$) or *Mlkl* (*Ptpn6*$^{\Delta PMN}$*Mlkl*$^{-/-}$), or the apoptotic arm by deletion of *Casp8* (*Ptpn6*$^{\Delta PMN}$*Casp8*$^{\Delta PMN}$) in *Ptpn6*$^{\Delta PMN}$ mice, was not sufficient to suppress inflammation (Fig. 2b). However, inhibition of both arms of cell death signaling in cohorts of *Ptpn6*$^{\Delta PMN}$*Casp8*$^{\Delta PMN}$*Ripk3*$^{-/-}$and *Ptpn6*$^{\Delta PMN}$*Casp8*$^{\Delta PMN}$*Mlkl*$^{-/-}$ mice resulted in a significantly reduced incidence of inflammation (Fig. 2b), as did deficiency in Ripk3, Mlkl and caspase-8 (*Ptpn6*$^{\Delta PMN}$*Casp8*$^{\Delta PMN}$*Ripk3*$^{-/-}$*Mlkl*$^{-/-}$) that achieved even greater protection. These data indicate that caspase-8- and Ripk3/Mlkl-dependent cell death pathways are individually capable of driving sufficient IL-1 release to promote disease in the absence of Ptpn6. Hence, deletion of both cell death pathways is required to limit the incidence of disease and delay the onset of IL-1-dependent footpad inflammation.

To answer whether the difference in disease onset between *Ptpn6*$^{\Delta PMN}$*Casp8*$^{\Delta PMN}$*Mlkl*$^{-/-}$ and *Ptpn6*$^{\Delta PMN}$*Casp8*$^{\Delta PMN}$*Ripk3*$^{-/-}$*Mlkl*$^{-/-}$ mice was a consequence of possible transcriptional effects mediated by Ripk3,[26] we performed RNA-Seq on neutrophils (Fig. 2c and Extended Data 1). We identified 3 dominant groups by k-means clustering, with group 3 being significantly enriched in *Ptpn6*$^{\Delta PMN}$ neutrophils (p=0.00046, Fisher's Exact test). Within group 3, there were no major differences in the transcriptome of *Ptpn6*$^{\Delta PMN}$ neutrophils lacking *Casp8*, *Ripk3*, or *Mlkl*. These data suggest that Ripk3 may promote cell death to release IL-1 and drive inflammation, in part, via a pathway independent of Mlkl and transcriptional changes in neutrophils. Gene Set Enrichment Analysis (GSEA) of the *Ptpn6*$^{\Delta PMN}$ samples in group 3 demonstrated an enrichment of genes in pathways consistent with activation of TNF, IL-6, and interferons in all genotypes (Fig. 2c and Extended Data 1). Further analysis of expression profiles from *Ptpn6*$^{\Delta PMN}$ neutrophils revealed a correlation between age and gene signature independent of the *Ripk3* and *Mlkl* genotypes (Extended

Data 1b, p=0.004, Group 1 v Group 2, Mann-Whitney test). Altogether, these data indicate that the disease process is driven by at least two distinct processes: a transcription-dependent change in *Ptpn6*$^{\Delta PMN}$ neutrophils that is not influenced by *Ripk3* loss, and a cell death-dependent process that releases IL-1 from neutrophils.

Ripk1 negatively regulates cutaneous inflammation

Numerous studies have reported that Ripk1 acts as a physiological negative regulator of both caspase-8-mediated apoptosis and Ripk3-Mlkl-mediated necroptosis *in vivo*.[19,22,23] To study the role of Ripk1 specifically in neutrophils, and gauge its role in the cutaneous inflammation seen in Ptpn6-deficient mice, we monitored disease progression in *Ptpn6*$^{\Delta PMN}$*Ripk1*$^{\Delta PMN}$ mice, where deletion of conditional *Ptpn6* and *Ripk1* alleles is restricted to neutrophils.[13] In further support of a role for Ripk1 in limiting the caspase-8-dependent apoptotic and Ripk3-Mlkl-dependent necroptotic cell death that drive this disease, *Ptpn6*$^{\Delta PMN}$*Ripk1*$^{\Delta PMN}$ mice developed cutaneous inflammatory disease with 100% penetrance, and at an accelerated rate compared to *Ptpn6*$^{\Delta PMN}$ mice (Figure 2b). The incidence of footpad inflammation in *Ptpn6*$^{\Delta PMN}$*Ripk1*^{D138N} mice, expressing a kinase dead form of Ripk1, was also 100% penetrant and accelerated compared to *Ptpn6*$^{\Delta PMN}$ mice (Figure 2b). These data suggest that Ripk1 kinase activity is engaged in the disease process, but that the absence of Ripk1, or its kinase activity, can still trigger an alternate caspase-8- or Ripk3-Mlkl-dependent inflammatory cell death pathway resulting in IL-1 release.

To further explore the role of Ripk1 activity *in vivo*, and to avoid perinatal lethality, we generated lethally irradiated chimeric mice containing *Ptpn6*$^{mev/mev}$ (n=6), *Ripk1*$^{-/-}$ (n=16), *Ptpn6*$^{mev/mev}$*Ripk1*$^{-/-}$ (n=11) or wild-type (n=10) fetal liver cells. *Ptpn6*$^{mev/mev}$*Ripk1*$^{-/-}$ fetal liver chimeric animals were devoid of cutaneous inflammatory disease and survived longer than *Ptpn6*$^{mev/mev}$*Ripk1*$^{+/+}$ fetal liver chimeric controls (Figure 3a), suggesting that Ripk1 may drive inflammation. However, analysis of the engraftment efficiency in *Ptpn6*$^{mev/mev}$*Ripk1*$^{-/-}$ and *Ptpn6*$^{+/+}$*Ripk1*$^{-/-}$ fetal liver chimeric mice at 12-weeks post-transplant by flow cytometry revealed a near complete absence of donor hematopoietic cells (Figure 3b) and hematopoietic progenitor cells (Figure 3c, Extended Data 2) in these animals. Thus, the absence of inflammation in *Ptpn6*$^{mev/mev}$*Ripk1*$^{-/-}$ fetal liver chimeric mice can instead be attributed to the known essential role of Ripk1 in hematopoietic engraftment[19,27,28], rather than to Ripk1 acting as a positive regulator of IL-1R-dependent inflammatory disease in this setting.

The exacerbated disease phenotype seen in *Ptpn6*$^{\Delta PMN}$*Ripk1*$^{\Delta PMN}$ mice suggests that loss of Ptpn6 may, in part, affect the ability of Ripk1 to negatively regulate inflammatory cell death. *Ptpn6*$^{\Delta PMN}$ neutrophils accumulated low-molecular weight Ripk1 isoforms, suggesting that disease may result from Ripk1 truncation and/or degradation leading to loss-of-function, rather than a spontaneous activation of Ripk1 kinase driving caspase-8 and Ripk3 activity (Figure 4a,b). Processing of Ripk1 was not dependent on caspase-8 in this context (Figure 4c). The rapid onset of disease in these mice lacking Ripk1 or Ripk1 kinase activity suggests that the nature of cell death regulation by Ripk1 in *Ptpn6*$^{\Delta PMN}$ neutrophils determines the scale of IL-1-mediated inflammation resulting from cell death.

Ripk1 prevents TNF-induced cell death in neutrophils

To understand why loss of Ripk1 in *Ptpn6*$^{\Delta PMN}$ neutrophils *in vivo* accelerated disease, we studied the response of wild-type, *Ptpn6*$^{\Delta PMN}$, *Ripk1*$^{\Delta PMN}$ and *Ptpn6*$^{\Delta PMN}$*Ripk1*$^{\Delta PMN}$ neutrophils to TNF stimulation *ex vivo*. To quantitatively track the rapid kinetic changes in neutrophil viability in response to apoptotic and necroptotic stimuli, we developed a live-cell imaging technique coupled to custom-scripted automated image analysis software (10.26180/5db913c24b884). Viability of neutrophils was tracked using Cell Tracker Green (CTG) to identify cells and track viability, Annexin V (AnnV) to identify cells undergoing apoptosis or necroptosis prior to membrane permeabilisation, and propidium iodide (PI) to identify dead cells (Figure 4d).[29,30] This approach allowed for the continuous enumeration of cell populations over time, thereby eliminating assumptions about the kinetics of cell death elicited by diverse stimuli, as well as the need to identify the most appropriate timepoint for analysis. *Ripk1*$^{\Delta PMN}$ neutrophils were highly sensitive to TNF stimulation (Figure 4f, and Extended Data 3–5). z-VAD-fmk treatment of TNF-stimulated *Ripk1*$^{\Delta PMN}$ neutrophils partially inhibited cell death (odds ratio 1.02 v 0.94 for per-hour viability of *Ripk1*$^{\Delta PMN}$ over wild-type in z-VAD-fmk + TNF over TNF, $p < 0.0001$), suggesting that both caspase-8-dependent and caspase-8-independent cell death pathways contribute to rapid cell death of TNF-treated *Ripk1*$^{\Delta PMN}$ neutrophils (Figure 4e, f, Extended Data 3–5, Supplementary Table 1). Birinapant treatment of TNF-stimulated wild-type neutrophils increased the kinetics of cell death to rates equivalent to those seen in TNF-stimulated *Ripk1*$^{\Delta PMN}$ neutrophils (OR 1.07 v 0.94, *Ripk1*$^{\Delta PMN}$ versus wild-type in BPT + TNF versus TNF, $p < 0.0001$, Extended Data 3–5). Birinapant/z-VAD-fmk-induced necroptotic cell death increased the ratio of CTG-AnnV+PI+ : CTG+AnnV+PI+ cell populations compared to birinapant-treated apoptotic wild-type neutrophils (Figure 4e and Extended Data 3). Importantly, *Ptpn6*$^{\Delta PMN}$*Ripk1*$^{\Delta PMN}$ neutrophils were also highly sensitive to TNF stimulation, with reductions in cell viability occurring with the same kinetics as *Ripk1*$^{\Delta PMN}$ neutrophils (Extended Data 3). Using an adapted imaging strategy, we also found that *Ripk1*$^{\Delta PMN}$ and *Ptpn6*$^{\Delta PMN}$*Ripk1*$^{\Delta PMN}$ neutrophils displayed elevated caspase-3/7 activation in response to TNF, and remained capable of undergoing non-apoptotic cell death in response to TNF+zVAD (Extended Data 4). Together, these data support a role for Ripk1 loss in sensitizing *Ptpn6*$^{\Delta PMN}$ neutrophils to cell death triggered by inflammatory cytokines, such as TNF.

IL-1α and IL-1β promote inflammatory disease

Prior studies support a key role for IL-1α in the disease process, contributing to footpad inflammation and impairing wound repair in *Ptpn6*$^{Y208N/Y208N}$ mice.[27] To address whether IL-1α is the exclusive regulator of spontaneous inflammatory disease in *Ptpn6*$^{Y208N/Y208N}$ mice, we generated *Ptpn6*$^{Y208N/Y208N}$*Il1a*$^{-/-}$ mice. In agreement with previous studies,[16,27] we found that IL-1α-deficiency does reduce the incidence of inflammatory disease (Figure 5a). However, this rescue was not complete, as only 50% of animals were protected. Loss of a single allele of *Il1a* (*Ptpn6*$^{Y208N/Y208N}$*Il1a*$^{-/+}$) gave similar levels of protection, implying sensitivity to changes in IL-1R signaling. To examine potential roles for IL-1β *in vivo*, we isolated neutrophils from the bone marrow and feet of inflamed *Ptpn6*$^{\Delta PMN}$ mice. Immunoblot of lysates revealed that pro-IL-1β was expressed in neutrophils isolated from the feet, but not the bone marrow, of *Ptpn6*$^{\Delta PMN}$ mice (Figure 5b), suggesting that IL-1β is

expressed and released from neutrophils at the site of inflammation. Consistent with previous reports that TLR ligands induce high levels of pro-IL-1β and IL-1α in *Ptpn6*$^{Y208N/Y208N}$ neutrophils[12], we observed elevated levels of IL-1α/β in cultured bone marrow neutrophils from *Ptpn6*$^{\Delta PMN}$ and *Ptpn6*$^{\Delta PMN}$*Ripk1*$^{\Delta PMN}$ mice, suggesting that neutrophils may act as a primary source of IL-1α/β in cutaneous inflammatory disease *in vivo* independently of Ripk1 (Figure 5c, d, e). Taken together, these new genetic data indicate that, while IL-1α may play a key role in wound repair, it is not the sole contributor to spontaneous IL-1R-dependent inflammation in *Ptpn6*$^{Y208N/Y208N}$ mice, thereby also implicating the other IL-1 family member that binds the IL-1R, IL-1β, in disease.[11,12]

Ptpn6 suppresses IL-1 secretion by necroptotic neutrophils

We originally demonstrated that IL-1R signaling was essential for cutaneous inflammatory disease in *Ptpn6*$^{Y208N/Y208N}$ mice.[11] Increased TLR-induced IL-1α and IL-1β production in *Ptpn6*$^{Y208N/Y208N}$ neutrophils was reported, however, the mechanism of IL-1α/β release was not established. Because *Ptpn6*$^{\Delta PMN}$ neutrophils display increased caspase-8- and Ripk3/Mlkl-dependent cell death in response to birinapant/z-VAD-fmk, we hypothesized that the increased sensitivity of *Ptpn6*$^{\Delta PMN}$ neutrophils to necroptotic stimuli could contribute to increased IL-1α and IL-1β secretion. Indeed, we observed increased levels of IL-1α and IL-1β in the supernatant of *Ptpn6*$^{\Delta PMN}$ neutrophils after a 16 h incubation with birinapant/z-VAD-fmk (Figure 5e). In addition, multiple isoforms of IL-1α and IL-1β were present in the supernatant, including full-length, and processed forms of approximately 17 kDa and 25 kDa, the latter of which is consistent with a bioactive form that can be generated in neutrophils by proteinase-3.[31] Priming of *Ptpn6*$^{\Delta PMN}$ neutrophils with the TLR2/6 ligand Pam_2CSK_4 further increased IL-1α and IL-1β release upon birinapant/z-VAD-fmk treatment, showing the propensity for necroptotic signaling to cause inflammation upon exposure of Ptpn6-deficient neutrophils to bacterial ligands. Caspase inhibition in TLR-primed neutrophils did not result in cell death, demonstrating a fundamental difference to macrophages under similar conditions (Figure 5f).[32]

The induction of IL-1 release associated with neutrophil cell death of birinapant/zVAD-fmk-treated cells was associated with the detection of phosphorylated Mlkl (pMlkl) (Figure 5g). This contrasts with the cleaved form of caspase-8 (cl.Casp8) appearing in freshly-isolated bone marrow *Ptpn6*$^{\Delta PMN}$ neutrophils, emphasizing the key roles of both caspase-8 and Ripk3/Mlkl in the disease process. These data also support dual roles for Ptpn6 in controlling the production of IL-1α/β at early time points following IAP depletion upon addition of a SMAC mimetic, and then IL-1α/β processing and/or secretion via caspase-8-dependent or Ripk3/Mlkl-dependent cell death at later timepoints.

Spontaneous TNF production in Ptpn6-deficient neutrophils does not require Ripk1

Induction of neutrophil necroptotic cell death by birinapant/z-VAD-fmk relies on autocrine or paracrine tumor necrosis factor (TNF) production, and is typically dependent on the kinase activity of Ripk1(Figure 6a).[33] To investigate the regulation of TNF production by Ptpn6, neutrophils derived from wild-type, *Ripk1*$^{\Delta PMN}$, *Ptpn6*$^{\Delta PMN}$, and *Ptpn6*$^{\Delta PMN}$*Ripk1*$^{\Delta PMN}$ mice were treated with birinapant/z-VAD-fmk to induce necroptosis and TNF secretion was measured. Induction of TNF production was markedly enhanced in

Ptpn6$^{\Delta PMN}$ neutrophils independently of Ripk1, with the exception of birinapant and birinapant/zVAD-fmk treatment (Figure 6b). These data indicate a critical role for Ptpn6 in controlling signaling events leading to TNF production. The fact that Ripk1 loss did not abrogate the spontaneous TNF secretion by *Ptpn6*$^{\Delta PMN}$*Ripk1*$^{\Delta PMN}$ neutrophils indicates that Ptpn6 deficiency circumvents the absolute requirement for Ripk1 kinase activity in maximal TNF production by neutrophils.

Spontaneous TNF and IL-1 production requires p38

The activity of p38 MAP kinase activity (marked by phosphorylation) is known to regulate Ripk1 inflammatory signaling in macrophages and fibroblasts[34–37]. We, and others, have observed that Ptpn6 deficiency in neutrophils results in an increase in p38 MAP kinase activity.[12,38] To examine the role of p38 MAP kinase in cytokine production and cell death signaling, we used the pan-p38 MAP kinase inhibitor BIRB-796 and the p38α/β-specific inhibitors, SB202190 and SB203580. Inhibition of p38 MAP kinase signaling by BIRB-796 completely abrogated both Ripk1-dependent and independent TNF production by *Ptpn6*$^{\Delta PMN}$ and wild-type neutrophils (Figure 6b), as well as pro-IL-1β production (Figure 6c). Together, these data indicate a Ripk1-independent role for Ptpn6 in the negative regulation of p38 MAP kinase signaling in neutrophils, leading to suppression of both TNF and IL-1 production.

p38 promotes neutrophil cell death

Given that inhibition of p38 signaling completely blocked TNF and IL-1 production in neutrophils, we hypothesized that it would also impede cell death. BIRB-796 completely inhibited necroptotic signaling of wild-type neutrophils equivalent to treatment with necrostatin-1s, while SB202190 and SB203580 had no effect (Figure 6d). These data implicate the p38-delta isoform, which is highly expressed in neutrophils[39] and inhibited by BIRB-796, in the regulation of neutrophil lifespan. To examine the effects of p38 MAP kinase inhibition in more detail, we used our live-cell imaging method to study kinetic changes in the cell death profile of neutrophils treated with BIRB-796. BIRB-796 impeded cell death of G-CSF-treated wild-type and *Ptpn6*$^{\Delta PMN}$ neutrophils (Figure 6e). Additionally, BIRB-796 inhibited Ripk3/Mlkl-dependent necroptotic death of wild-type and *Ptpn6*$^{\Delta PMN}$ neutrophils treated with birinapant/zVAD-fmk (Figure 6f). Addition of BIRB-796 led to both slower death kinetics and a reduction in phosphatidylserine exposure on the plasma membrane, an early event in both apoptotic and necroptotic cell death marked by Annexin V staining[29,30], in both wild-type and *Ptpn6*$^{\Delta PMN}$ neutrophils (Figure 6e,f). Membrane permeabilization was also delayed in response to BIRB-796, as measured by the appearance of PI-positive cells, (Figure 6f). These data suggest that p38 MAP kinase signaling is involved in both the G-CSF-regulated apoptotic, and the Ripk3-Mlkl-regulated necroptotic cell death pathways and, thus, controls both IL-1 production and release by neutrophils.

Ptpn6 Y208N mutation prevents its interaction with myosin-9 in neutrophils

This study has largely examined the effect of Ptpn6 deficiency on neutrophil function, however, why mutant forms of Ptpn6 also fail to repress IL-1R-dependent cutaneous inflammatory disease remain to be fully elucidated, such as is the case for *Ptpn6*$^{Y208N/Y208N}$ neutrophils.[12] We therefore explored the nature of the binding interactions of the C-terminal

SH2 (C-SH2) domain of Ptpn6. The Ptpn6 C-SH2 domain harbours the Y208N mutation, and the effect of this mutation on coordinating the exposure of pY and pY+3 residues on substrates is unclear. To examine possible structural changes induced by the Y208N mutation, we investigated the interaction between the NKG2A peptide interaction motif and the Ptpn6 C-SH2 domain using the solution structure of the complex (PDB: 2YU7). This indicated that Y208 is located outside of the pY and pY+3 binding pockets of the C-SH2 domain, and is unlikely to make any contact with any pY-containing substrates (Figure 7a). These data suggest that the Y208N mutation influences Ptpn6 function independently of its ability to bind to phosphorylated motifs in protein substrates.

To identify changes in interacting partners caused by the Y208N mutation in neutrophils, we generated biotinylated wild-type or Y208N peptides corresponding to sequence from the C-SH2 domain of Ptpn6. Immunoprecipitation of interacting partners with these biotinylated peptides, followed by mass spectrometry of candidate proteins, revealed that Y208N peptides failed to interact, or had a greatly reduced interaction, with myosin-9 and actin (Figure 7b,c and Supplementary Table 2). These data suggest that the Y208 motif, adjacent to the BG loop of the C-SH2 domain, is essential for interaction of Ptpn6 with myosin-9. Studies using isothermal titration calorimetry indicated that the mutant Ptpn6 Y208N C-SH2 domain was not compromised in its ability to bind tyrosine-phosphorylated peptides from FcγR2b, a known substrate for Ptpn6 (Ptpn6 Y208N C-SH2 domain: K_D 10.4 μM; Ptpn6 wt C-SH2 domain: K_D 20.1 μM) (Figure 7d). Thus, the motif containing Y208 likely contributes to the stabilization of Ptpn6 protein via interactions with the actin-myosin-9 cytoskeleton rather than ITIM motif interactions. This Y208-myosin-9 interaction likely prevents degradation of mislocalized Ptpn6, as evidenced by reduced $Ptpn6^{Y208N}$ protein in neutrophils[12], and may indirectly facilitate negative regulation of signal transduction and cell death complexes within the neutrophil. New genetic tools targeting the cell death signaling cascade will be needed to better characterize these regulatory networks in neutrophils.

DISCUSSION

These data support a dual action model of Ptpn6 function to suppress IL-1R-dependent disease: the first, inhibiting p38 MAP kinase function to limit TNF and IL-1α/β production; and the second, control of Ripk1 function to inhibit apoptotic and necroptotic neutrophil cell death and IL-1 release. The capacity of neutrophils to access either caspase-8-dependent apoptotic signaling, or Ripk3/Mlkl-dependent necroptotic signaling, is consistent with the role of Ripk1 in coordinating cell death based on the availability of caspase-8 and Ripk3/Mlkl substrates.[33,40,41] Cell death and IL-1α/β release may also be influenced *in vivo* by TLR-dependent degradation of cIAP1, depletion of IAPs in response to apoptotic stimuli, or an inability to dephosphorylate caspase-8 at Y397 and Y465 due to Ptpn6 deficiency.[42–44]

Ptpn6 regulation of p38 MAPK activity appears central to the disease process. Suppression of p38 MAPK activity in $Ptpn6^{\Delta PMN}$ neutrophils impairs IL-1α/β and TNF production, but also blocks apoptotic and necroptotic cell death. This is in stark contrast to the scenario in macrophages and fibroblasts that can become sensitized to TNF-induced Ripk1-regulated

cell death upon p38 MAPK inhibition, demonstrating cell-type specific roles for p38 MAPK in cell death signaling.[34–37]

The loss of Ripk1 function in *Ptpn6*$^{\Delta PMN}$*Ripk1*$^{\Delta PMN}$ mice increases the incidence and accelerates the onset of footpad inflammation. Unexpectedly *Ptpn6*$^{\Delta PMN}$*Ripk1*$^{\Delta PMN/D138N}$ mice were also sensitized to development of spontaneous inflammatory disease. These data indicate that Ripk1 kinase activity is engaged in *Ptpn6*$^{\Delta PMN}$ neutrophils, but suggest that the scaffolding function of Ripk1 may be defective due to changes in death domain (DD) and RHIM domain function in full-length and/or low M_W isoforms of Ripk1. The exacerbation of the cell death phenotype in *Ptpn6*$^{\Delta PMN}$*Ripk1*$^{\Delta PMN}$ mice is consistent with the ability of necroptotic and caspase-8-dependent apoptotic cell death to proceed in the absence of Ripk1.[19,22,23] In the absence of Ripk1, tumor necrosis factor receptor type I-associated death domain protein (TRADD) has been shown to complex with caspase-8/cFLIP/FADD via DD interactions to drive systemic inflammation and apoptotic cell death independently of Ripk3.[45,46] In an analogous manner, the absence of the RIP homotypic interaction motif (RHIM) domain of Ripk1 enables Z-DNA binding protein 1 (ZBP1) to complex with Ripk3 to drive Mlkl-dependent necroptosis.[47] The increase in truncated Ripk1 isoforms in *Ptpn6*$^{\Delta PMN}$ mice, and associated loss of Ripk1 regulatory function, may therefore enable the recruitment of TRADD to complexes of caspase-8/cFLIP/FADD, and recruitment of ZBP1 to Ripk3 (Fig. 4a,b and Extended Data Fig. 6). Future studies in Ptpn6-deficient macrophages may enable a complete picture of Ptpn6 function in these pathways to be generated.

Ptpn6 deficiency triggers IL-1R-dependent disease via neutrophil cell death but the extrinsic factors accelerating disease progression are not well defined. Prior studies demonstrate that TNF contributes to lethality in *Ripk1*$^{-/-}$, *Casp8*$^{-/-}$, *cFlip*$^{-/-}$, *cIAP1*$^{-/-}$*cIAP2*$^{-/-}$, and *Fadd*$^{-/-}$ embryos and neonates.[19,22,23,48,49] The loss of Ptpn6 itself is associated with a reduction in full-length Ripk1 protein that may promote cell death. What cell-extrinsic factors promote IL-1 release and cell death *in vivo* remain to be determined, but TNF likely plays a role.[16,17] These data do not exclude a role for non-hematopoietic cells in the generation of, or response to, IL-1α/β, but they strongly support a primary role for neutrophils in both the production and release of IL-1α/β in cutaneous inflammation.

Ptpn6 can interact with actin to regulate the conversion of mechanical forces, controlled by the actomyosin network, into biochemical signals.[50] In this setting, changes in actin dynamics control the catalytic activity of Ptpn6. Our finding that the Y208N mutation prevents association of Ptpn6 with myosin-9 supports these data in neutrophils, and may have unexpected outcomes on negative regulation of specific TLR and cell death signaling cascades in neutrophils, including those controlling low M_W Ripk1 isoforms and Ripk1 function.

Ptpn6 has been extensively implicated in human inflammatory disease, autoimmunity, and cancer. Our findings suggest that one of the dominant roles of Ptpn6 may be as a negative regulator of inflammatory cell death pathways. Defects in cell death may also underlie IL-1R-dependent pneumonitis in *Ptpn6*$^{me/me}$ mice, and predispose patients with neutrophilic dermatoses expressing *PTPN6* coding and transcript variants to autoimmunity and leukemia.

METHODS

Mice

The *Ptpn6*$^{\Delta S100a8Cre/\Delta S100a8Cre}$ (*Ptpn6*$^{\Delta PMN}$),[51] *Ptpn6*^{Y208N},[11] *Ptpn6*^{mev},[52] *Ripk1*$^{+/-}$,[53] *Ripk1*$^{-/\Delta S100a8Cre}$ (*Ripk1*$^{\Delta PMN}$),[54] *Ripk1*$^{-/D138N}$ (*Ripk1*^{D138N}),[55] *Ripk3*$^{-/-}$,[56] *Caspase-8*$^{\Delta S100a8Cre/\Delta S100a8Cre}$ (*Casp8*$^{\Delta PMN}$),[57] and *Mlkl*$^{-/-}$ [58] mouse strains were generated on or had been backcrossed at least 10 generations with the C57BL/6J background. All animal experiments complied with the regulatory standards of, and were approved by the Institutional Animal Care and Use Committee at Boston Children's Hospital and The Walter and Eliza Hall Institute of Medical Research. Mice were housed under specific pathogen-free conditions with unlimited access to food and water.

Bone marrow neutrophil purification

Murine bone marrow cells were isolated from the femur, tibia, and ossa coxae in Hanks Balanced Salt Solution supplemented with 1% fetal bovine serum (FBS) and 15 mM EDTA. Cells were overlayed on 78%, 68% and 52% Percoll layers and centrifuged at 400 × g for 30 min at 4 °C. Neutrophils were removed from the 68%/78% interface and re-suspended in DMEM/10% FBS for biochemical assays, DMEM/0.5% FBS for IL-1α/β immunoblot assays, or phenol red-free DMEM/10% FBS for live cell imaging viability assays. The purity of neutrophil preparations was typically greater than 95% as assessed by May-Grünwald Giemsa staining. All cell culture medium were purchased from Gibco.

Viability assays

For induction of cell death, neutrophils were treated with 100 ng/mL recombinant human G-CSF (Amgen) or 100 ng/mL recombinant mouse IFN-γ (Peprotech), and then treated with combinations of 50 ng/mL recombinant mouse TNF (BioLegend), 2 μM Birinapant (Tetralogic Pharmaceuticals), 10 μM z-VAD-fmk (Sigma), or 10 μM necrostatin-1s (Enzo Life Sciences). For some assays, neutrophils were primed with 100 ng/mL recombinant mouse IFN-γ and 10 ng/mL Pam_2CSK_4 (Invivogen). The p38 MAP kinase inhibitors BIRB-796, SB202190 and SB203580 (EMD Millipore) were used at a final concentration of 20 μM.

Live-cell imaging

Neutrophils were labeled with 200 nM CellTracker Green or 100 nM CellTracker Orange (Life Technologies) for 15 min at 37 °C in serum-free DMEM. 1×10^5 neutrophils were plated in PureCoat Amine 96 well optical bottom plates (Corning). Neutrophil viability was monitored using AnnexinV-AlexaFluor647 (BioLegend) to detect phosphatidylserine, CellEvent Caspase-3/7 Detection Reagent, 0.5 μg/mL propidium iodide, or Draq7 according to the manufacturer's instructions (BioLegend). Images from triplicate fields of view were captured at 10 × at 37ºC + 5% CO_2 every hour by the ImageXpress Micro Confocal High-Content Imaging System (Molecular Devices) operating MetaXpress (Version 6.2.5) acquisition software. Three non-overlapping 1.96 mm^2 zones within each well were imaged for red, green and far-red fluorescence (excitation/emission at 531/593, 475/536 and 634/692 nm, respectively). Cell death kinetics were analyzed using a custom macro in the Fiji

distribution of ImageJ.[59] The macro processed each timepoint folder that was generated by the ImageXpress imaging system, and time image stacks were constructed of each well field position. The macro segmented each cell population in each frame of the time stacks using watershed segmentation, and then population percentages were calculated for each time point from the extracted binary images. At each time point, the cells in each channel (Cell Tracker Green, propidium iodide, and Annexin V) were extracted by applying a Gaussian Blur (sigma =2 for full resolution data, sigma =1 for binned data) and then using standard watershed segmentation to generate binary images representing each cell. Using these masks, each cell population was defined using Boolean arithmetic. The logic was constructed so that cells were only counted once. Data was logged and percentage populations were calculated at each time point. The CTG-AnnV-PI+ population did not meet the criteria of a cell and were excluded from all analyses.

Immunoblot

Neutrophils were lysed in 1% (v/v) Triton X-100, 1% (w/v) sodium deoxycholate, 0.1% (w/v) SDS, 10 mM NaF, 1 mM sodium vanadate, 1 mM phenylmethanesulphonylfluoride in 10 mM Tris-HCl, pH 7.5, 150 mM NaCl and Complete Protease Inhibitor Cocktail (Roche). Cell lysates and supernatants were analyzed using antibodies specific to IL-1β/IL-1F2 (R&D; AF-401), IL-1α/IL-1F1 (R&D; AF-400), RIPK1 (Cell Signaling Technology; D94C12), SHP-1 (Cell Signaling Technology; C14H6), p38 MAPK (Cell Signaling Technology; D94C12), phospho-p38 MAPK (T180/Y182) (Cell Signaling Technology; 9211), Myosin-9 (Cell Signaling, #3403), p42/44 MAPK (ERK1/2) (Cell Signaling Technology; 137F5), or phospho-MLKL (S345) (Abcam; EPR9515[2]). Westerns were developed (ECL Substrate), visualized (ChemiDoc), and analyzed (ImageLab Software) with BioRad products.

Enzyme-linked immunosorbent assay (ELISA)

The Mouse TNF ELISA kit by Thermofisher (Cat. # 88–7324) was used according to the manufacturer’s instructions.

Flow cytometry

Flow cytometry analysis was performed on a LSRII or LSRFortessa (BD Biosciences). To isolate neutrophils from the feet, tissue was diced and incubated at 37°C for 45 min with shaking at 200 rpm (TissueLyserII, Qiagen), in DMEM containing 1 mg/mL Collagenase Type IV (Worthington Biochemical). Cells were then strained through a 70 μM strainer and washed twice in phosphate buffered saline (PBS). Neutrophils from bone marrow and feet were sorted on a FACSAria III (BD Biosciences). FcγR were blocked using TruStain FcX (BioLegend). Data were analyzed using FlowJo software (BD Biosciences). The following reagents were used: Zombie-NIR fixable viability kit (BioLegend), anti-B220 (eBioscience;RA36B2), anti-CD3 (WEHI;KT3.1.1), anti-CD4 (WEHI;GK1.5), anti-CD8 (WEHI;53.6.7), anti-CD11b (BioLegend;M1/70), anti-CD16/32 (WEHI;24G2), anti-CD34 (eBioscience;RAM34), anti-CD45.1 (BioLegend;A20), anti-CD45.2 (BioLegend;104), anti-CD48 (BD Bioscience;C2), anti-CD127 (eBioscience;A7R34), anti-CD135 (BioLegend;A2F10), anti-CD150 (BioLegend;TC15–12F12.2), anti-cKit (WEHI;ACK4),

anti-Gr1 (WEHI;RB6–8C5), anti-Ly6G (BD;1A8), anti-Sca-1 (WEHI;Ly6A/E), anti-Siglec-F (Fisher;1RMN44N), AnnexinV-AF647 (BioLegend), and propidium iodide (Sigma).

Fetal liver chimeras

For experiments utilizing *Ripk1*$^{-/-}$ fetal liver cells, chimeric animals were generated by reconstituting lethally-irradiated (2×550R given 3 h apart) B6.SJL-*Ptprc*^{a} *Pepc*^{b}/BoyJ (Ly5.1)-expressing mice with 10^6 E13.5 fetal liver cells from wild-type, *Ptpn6*$^{mev/mev}$, *Ptpn6*$^{mev/mev}$ *Ripk1*$^{-/-}$ or *Ripk1*$^{-/-}$ embryos. Automated cell counts were performed on blood collected from the retro-orbital plexus into Microtainer tubes containing EDTA (Sarstedt) using an Advia 2120 hematological analyzer (Siemens). Peripheral blood and bone marrow chimerism were analyzed 12 weeks post-transplant using antibodies specific for CD45.1, CD45.2, CD16/32, CD48, CD127, CD135, CD150, cKit, Sca-1, CD4, CD8, Ly6G, Ly6C and CD11b on a BD LSRII flow cytometer and analyzed using FlowJo software. HSPC populations were gated as lineage-negative (lin-) cKit^{+} Sca1^{+} CD48^{-} CD150^{+} (HSC), lin^{-} cKit^{+} Sca1^{+} CD48^{+} CD150^{+} (MPP), lin^{-} cKit^{+} Sca1^{+} CD48^{+} CD150^{-} (LRP), lin^{-} cKit^{+} Sca1^{lo} CD16/32^{hi} (GMP), lin^{-} cKit^{+} Sca1^{lo} CD16/32^{lo} CD34^{+} (CMP), lin^{-} cKit^{+} Sca1^{lo} CD16/32^{lo} CD34^{-} (MEP), lin^{-} cKit^{int} Sca1^{lo} Flt3^{+} IL-7R^{+} (CLP).

Isothermal titration calorimetry

Isothermal calorimetric titrations were performed using a Microcal Omega VP-ITC (MicroCal Inc.). SHP1-SH2 (wild-type and Y208N) were dialysed against buffer (20 mM Tris, 100 mM NaCl, 2 mM 2-mercaptoethanol, pH 8.0) and the dialysis buffer used to prepare solutions of FcR, Fas, and IRAK phosphopeptides. Experiments were performed at 298 K. Typically, thirty 10 μl injections of phosphopeptide (100 μM) were titrated into a 10 μM solution of recombinant SHP1-C-SH2 protein. As only the FcR phosphopeptide bound SHP-1 those experiments were repeated using higher concentrations of protein and ligand (40 μM and 400 μM respectively) to obtain more accurate quantitative data. The heat of dilution of the phosphopeptide was subtracted from the raw data of the binding experiment. Data were analyzed using the evaluation software (Microcal Origin version 5.0). For the SHP-1/FcR interaction, the binding curves fitted a single-site binding mode and K_d values were determined from duplicate experiments.

Gel excision, digestion and Nano-LCMS/MS

For protein samples in gels, bands (~2 mm) were excised from the 1-D gel lane and subjected to automated in-gel reduction, alkylation, and tryptic digestion using the MassPREP Station (Micromass). The gel bands were reduced with 10 mM DTT (Calbiochem) for 30 min, alkylated for 30 min with 50 mM iodoacetic acid (Fluka) and digested with 375 ng trypsin (Worthington) for 16 h at 37 °C. The extracted peptide solutions (0.1% formic acid) were then concentrated to approximately 10 μL by centrifugal lyophilisation using a SpeedVac AES 1010 (Savant). Digested peptides were subjected to nano-liquid chromatography in conjunction with collisional tandem mass spectrometry (nano-LC-MS/MS). Briefly, extracted peptides were injected and fractionated by nanoflow reversed-phase liquid chromatography on a nano LC system (Agilent; 1200 series) using a nanoAcquity C18 150mm × 0.15 mm I.D. column (Waters) developed with a linear 60-min gradient with a flow rate of 0.5 μl/min at 45 °C from 100% solvent A (0.1% formic acid in

Milli-Q water) to 100% solvent B (0.1% formic acid, 60% acetonitrile [Mallinckrodt Baker], 40% Milli-Q water). The nano-HPLC was coupled on-line to an LTQ-Orbitrap mass spectrometer equipped with a nanoelectrospray ion source (Thermo Fisher Scientific) for automated MS/MS. Up to five most intense ions per cycle were fragmented and analyed in the linear trap, with target ions already selected for MS/MS being dynamically excluded for 3 min.

Mass spectra database searching, protein identification, bioinformatic and statistical analysis

Mass spectra peak lists were extracted using extract-msn as part of Bioworks 3.3.1 (Thermo Fisher Scientific) linked into Mascot Daemon (Matrix Science). The parameters used to generate the peak list for the Orbitrap were as follows: minimum mass 400; maximum mass 5000; grouping tolerance 0.01Da; intermediate scans1; minimum group count 1; 10 peaks minimum; and total ion current of 100. Peak lists for each nano-LC-MS/MS run were used to search MASCOT v2.2.04 search algorithm (Matrix Science) provided by the Australian Proteomics Computational Facility. Automatic charge state recognition was used because of the high-resolution survey scan (30000). LC-MS/MS files were searched against an extensive database using the following search parameters: carboxymethylation of cysteine as a fixed modification (+58Da) with variable modifications set for NH_2-terminal acetylation (+42Da) and oxidation of methionine (+16Da). A peptide mass tolerance of +/−20ppm, ^{13}C defined as 1, fragment ion mass tolerance of +/−0.8Da, and an allowance for up to three missed cleavages for tryptic searches where trypsin was used as the digest reagent. No-enzyme (unrestricted) searches were also carried out on all Orbitrap-LTQ data and manual validation of all peptide spectral matches was done irrespective of peptide scores or expectation values (E-values) to ensure that all major fragment ions were annotated in accordance with known rules of peptide fragmentation.

RNA-seq for transcriptome analysis

Total RNA was extracted from 10^6 bone marrow neutrophils according to the manufacturer's instructions (Qiagen). Paired-end sequencing was performed by BGI Americas, and read lengths were 100 base pairs (GEO record GSE139223). The total number of reads for each sample were between 48–52 × 10^6. RNA-Seq quality was assessed using fastqc[60], and there were no quality concerns from the analysis. Transcripts were quantified using Salmon[61] against the C57BL/6J mouse genome annotation Genome Reference Consortium Mouse Build 38 patch release 6 (GRCm38.p6), obtained from NCBI.

All statistical analysis was conducted using R v.3.5.1. Genes with less than an average of 3 reads per sample were discarded. Differentially expressed (DE) genes were determined using the DESeq2[62] pipeline with default parameters. Multiple hypothesis correction was done using the Benjamini-Hochberg method, and a p-adjusted value of 0.1 was considered significant.

To control for gender effects, all samples were obtained from female mice. To control for potential erythroid contamination of Percoll-purified neutrophils, we estimated the proportion of other bone marrow cells using the software Cibersort[63] and data from

Haemosphere.org (V4.9.5, dataset GSE116177). Briefly, reference samples are used, wherein each sample contains RNA data of pure cell types. These are used to create a gene signature matrix containing genes that best separate hematopoietic cell types. The proportion of each cell type is estimated using vector regression, and assumes that the mRNA mixture values are linear combinations of expression in each lineage. Analyzed samples contained less than 10% erythroid cells based on this analysis. Additionally, the erythroid proportion was used as a covariate in the differential expression design, accounting for any residual signature.

To generate heatmaps, counts were transformed using the variance stabilizing transform of DESeq2, which accounts for library size and removes heteroskedasticity of the counts. Additional samples were used for the transform to give a better account of the variance of the gene levels. These values were then z-scored gene-wise. Hierarchical clustering was performed using an average linkage method with euclidean distance as the metric.

To cluster the samples, the k-means algorithm in scikit-learn[64] was used with k=3 to cluster the samples based on their normalized gene expression values. The genes used were all genes that were differentially expressed in at least one comparison across genotypes.

To determine which pathways and gene sets were affecting the apparent grouping, Gene Set Enrichment Analysis (GSEA) was performed after running differential expression analysis for each group comparison.[65] GSEA finds gene sets whose genes are more significantly different across the groups. The Hallmark gene sets from the Molecular Signatures Database (MSigDB) were used. The Normalized Enrichment Score (NES) represents how much more enriched a gene set is compared to permutations of the expression dataset. The normalized enrichment score was computed using 1,000 permutations of the genes in the dataset, as described in the GSEA documentation. The Benjamin-Hocheberg corrected p-value of 0.1 was used, and a minimum of 20 genes were needed in the set.

Genotyping

Mice were genotyped with the following primers—*Ptpn6*^{Y208N}: 5′-ACGCTGGAGCTTCAGTGGAC-3′; 5′-TGAGGTGAGGGAGGACGA-3′. Amplicons were digested with HincII to distinguish wild-type and Y208N alleles.

S100a8-Cre:5′-CTGACCGTACACCAAAATTTGCCTG-3′;5′-GATAATCGCGAACATCTTCAGGTTC-3′

Il1a$^{-/-}$: 5′-AGACCATCCAACCCAGATCA-3′; 5′-CCAAGTGGTGCTGAGATAGTG-3′;

5′-CggAAgTgCTTgACATTgg-3′; 5′-gTATTgACCgATTCCTTgCg-3′

Ptpn6^{fl} 5′-ACCCTCCAGCTCCTCTTC-3′; 5′-TGAGGTCCCGGTGAAACC-3′

Mlkl$^{-/-}$: 5′-TATGACCATGGCAACTCACG-3’; 5’-ACCATCTCCCCAAACTGTGA-3’; 5’-TCCTTCCAGCACCTCGTAAT-3’

Ripk3$^{-/-}$: 5′-AGAAGATGCAGCAGCCTCAGCT-3’; 5′-ACGGACCCAGGCTGACTTATCTC-3’; 5′-GGCACGTGCACAGGAAATAGC-3’

Ripk1^{fl}: 5′-GGAGGCAATGAGAAGAAAACAGC-3’; 5′-GCATCGATCTGGCCTGATGAAG-3’

Ripk1$^{+/-}$: 5′-GAGCAATCAAAATGCAACCA-3’; 5′-tttatgcccccaactcacTC-3’; 5′-gaagcgggaagggactggctgcta-3’; 5′-cgggagcggcgataccgtaaagc-3’

Casp8^{fl}: 5′-CCAGGAAAAGATTTGTGTCTAGC-3’; 5′-GGCCTTCCTGAGTACTGTCACCTGT-3’

Ripk1^{D138N}: 5′-TCATCCCACCCTCATGAGTG-3’; 5′-GTCAAGCCTGCACCTTTCAT-3’. Amplicons were digested with AvaII to distinguish wild-type and D138N alleles.

GLIMMIX

For live cell image statistical analysis, the generalized linear mixed model (GLIMMIX) was utilized. Variables are assigned according to time *I,* well *j,* and cell number c_{ij}, in a transition state (or states) of interest, which are a subset of some total number d_{ij} of cells in the image. A generalized linear mixed model was fit to the outcome $Y_{ij} = c_{ij} / d_{ij}$, the proportion of cells of interest in well *i* at time *j*. Tg_i represents the treatment-genotype combination for well *i*. Then

$$logit\left\{E\left(Y_{ij}|b_i\right)\right\} = \beta_1 + \beta_2\, x\, time\left(j\right) + \beta_3\, x\, time\left(j\right) x\, Tg_i$$

Interwell correlation between genetic replicates is accounted for by Tg_i which specifies a fixed effect for each treatment-genotype combination. Define $b_i = c_{i1} / d_{i1}$, a random intercept, and a_i, a time slope, for well *i*, accounting for correlation of images of each well. Then given a_i and b_i it is assumed d_{ij} Y_{ij} are independent and binomial-distributed as bin(d_{ij}, $\boldsymbol{\pi}_{ij}$) with

$$Var\left(Y_{ij}\right) = \pi_{ij}\left(1 - \pi_{ij}\right)/d_{ij}$$

Precision is increased due to the ability to distinguish individual cells in each image in the live cell imaging technique: variance of a binomial outcome varies inversely with the denominator. Underestimation of the standard errors due to overdispersion is remedied by use of the classical empirical (“sandwich”) estimator of *Cov(β).*

Finally we assume the random effects a_i and b_i have a bivariate normal distribution with mean [0, 0], covariance σ^2_{ab}, and variances σ^2_a and σ^2_b, so $\begin{bmatrix} a_i \\ b_i \end{bmatrix} \sim \mathcal{N}\left(\begin{bmatrix} 0 \\ 0 \end{bmatrix}, \begin{bmatrix} \sigma^2_a & \sigma^2_{ab} \\ \sigma^2_{ab} & \sigma^2_b \end{bmatrix}\right)$. The model supposes each genetic replicate in a treatment has its own underlying probability of transitioning out of the state(s) of interest that does not vary over the course of the experiment.

All data preparation for and inference by GLIMMIX in this paper was performed with SAS 9.4 (SAS Institute, Cary, NC).

Statistics

Data are presented as mean ± standard error of the mean (SEM). Comparisons were performed using t tests, or ANOVA with a Tukey's multiple comparison test. Changes in disease-free survival were monitored using a Log-rank (Mantel-Cox) test.

Code availability

The custom-scripted macro used for automated image analysis of live cell imaging data is available from 10.26180/5db913c24b884.

Data availability

The data supporting the findings of this study are available within the manuscript and supplemental materials, and are available from the corresponding author upon request.

Extended Data

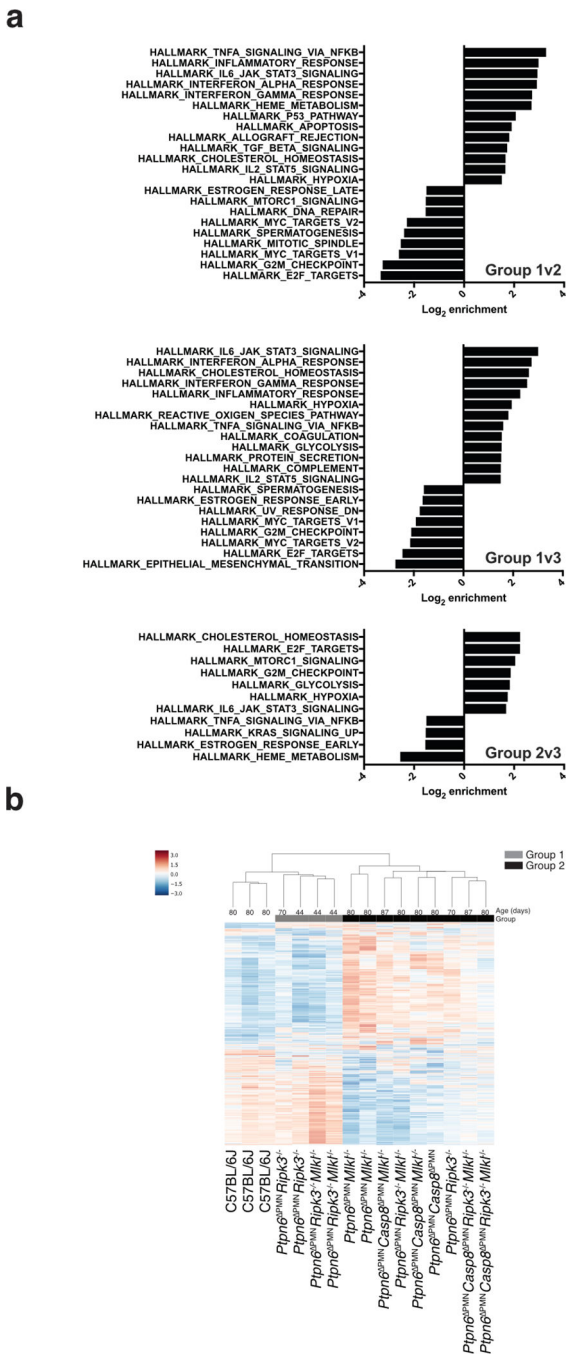

Extended Data 1. Ptpn6 prevents an inflammatory signature in bone marrow neutrophils.

a) Gene Set Enrichment Analysis of RNA-Seq transcriptomic data derived from bone marrow neutrophils of female *Ptpn6*$^{\Delta PMN}$*caspase-8*$^{\Delta PMN}$*Ripk3*$^{-/-}$*Mlkl*$^{-/-}$ mice and controls.

b) Age-dependent effects on the neutrophil transcriptome in *Ptpn6*$^{\Delta PMN}$*caspase-8*$^{\Delta PMN}$*Ripk3*$^{-/-}$*Mlkl*$^{-/-}$ mice and controls.

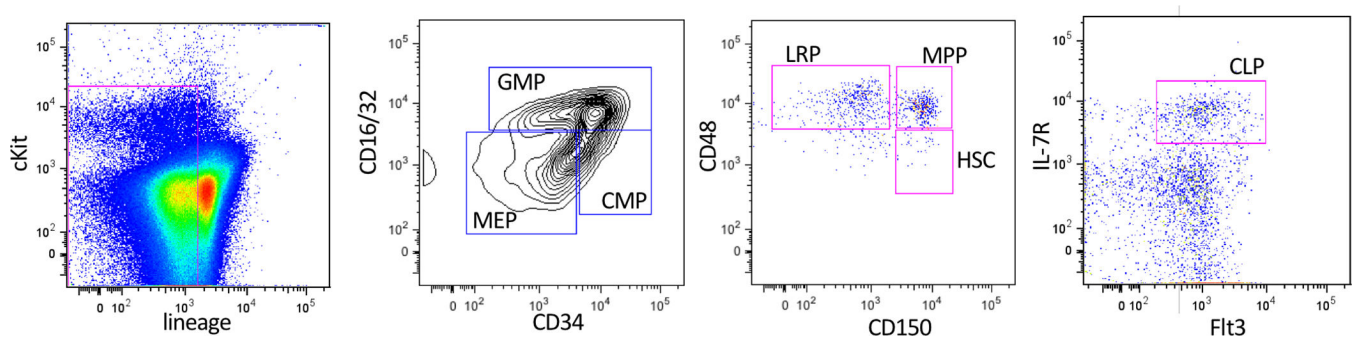

Extended Data 2. Flow cytometry gating strategy for hematopoietic stem and progenitor cells (HSPC).

For gating of HSPC in Figure 3, bone marrow cells were sorted after enrichment for hematopoietic progenitor cells by magnetic bead-based depletion of lineage-positive hematopoietic cells. (a) Definition and gating strategy for lineage restricted progenitors (LRP), multi-potent progenitors (MPP), and hematopoietic stem cells (HSC), (b) common myeloid progenitors (CMP), megakaryocyte erythroid progenitors (MEP), granulocyte macrophage progenitors (GMP), and (c) common lymphoid progenitors. Lineage-negative cells and gating were defined using isotype control antibodies.

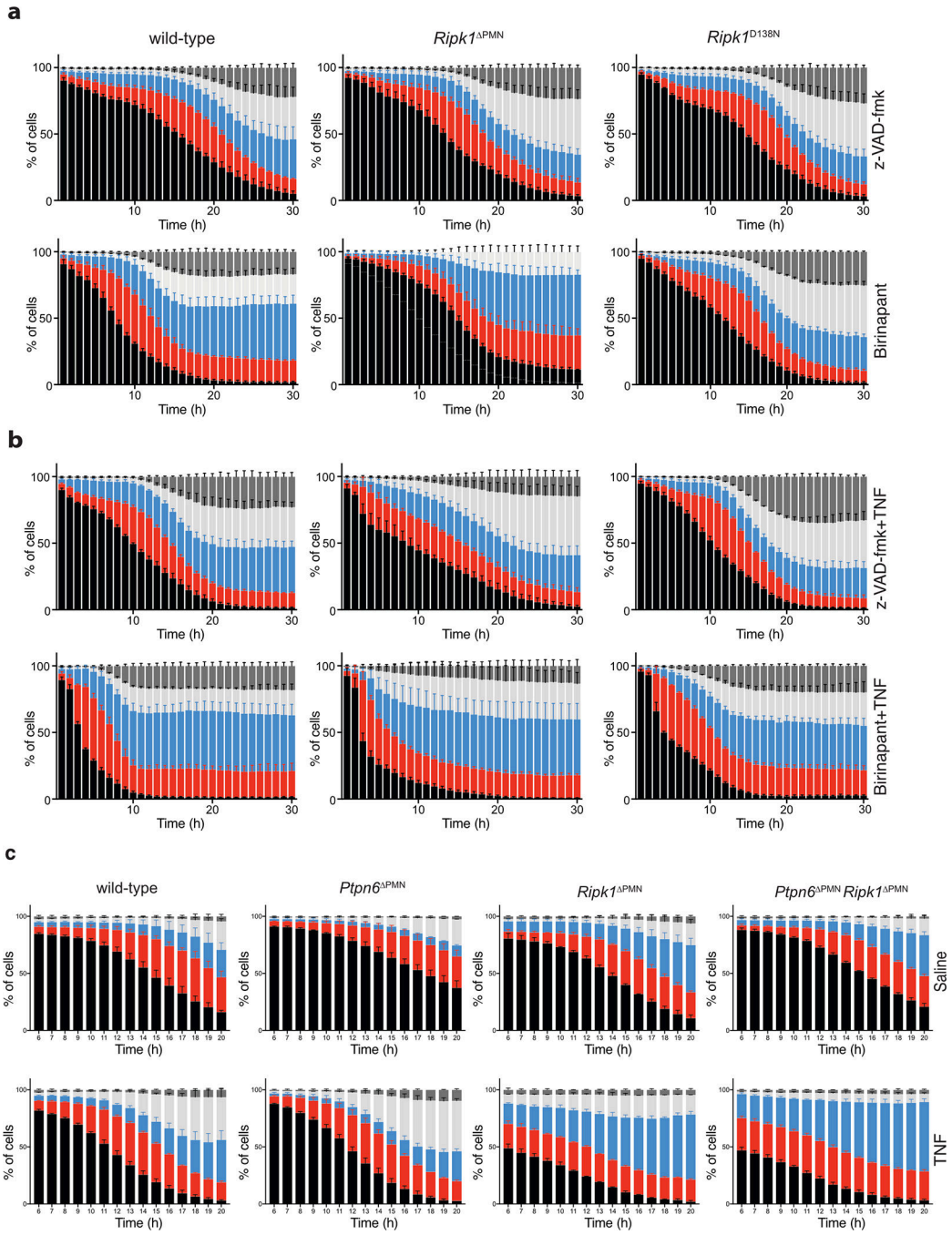

Extended Data 3. Loss of RIPK1 sensitizes neutrophils to TNF-mediated cell death.

a-b) Live-cell imaging of CTG-labeled wild-type, *Ripk1*$^{\Delta PMN}$, and *Ripk1*$^{D138N/D138N}$ neutrophils treated with 2 μM BPT and/or 10 μM z-VAD-fmk +/− 100 ng/mL TNFα. PI and Annexin V were used to monitor changes in viability. Mean and SEM, n=3 biologically independent samples, and triplicate fields of view per independent biological sample. **c)** Live-cell imaging of CTG-labeled wild-type, *Ptpn6*$^{\Delta PMN}$, *Ripk1*$^{\Delta PMN}$, and *Ptpn6*$^{\Delta PMN}$*Ripk1*$^{\Delta PMN}$ neutrophils treated with saline or 100 ng/mL TNFα. PI and Annexin

V were used to monitor changes in viability. Mean and SEM of technical replicates shown. Data are representative of two independent experiments.

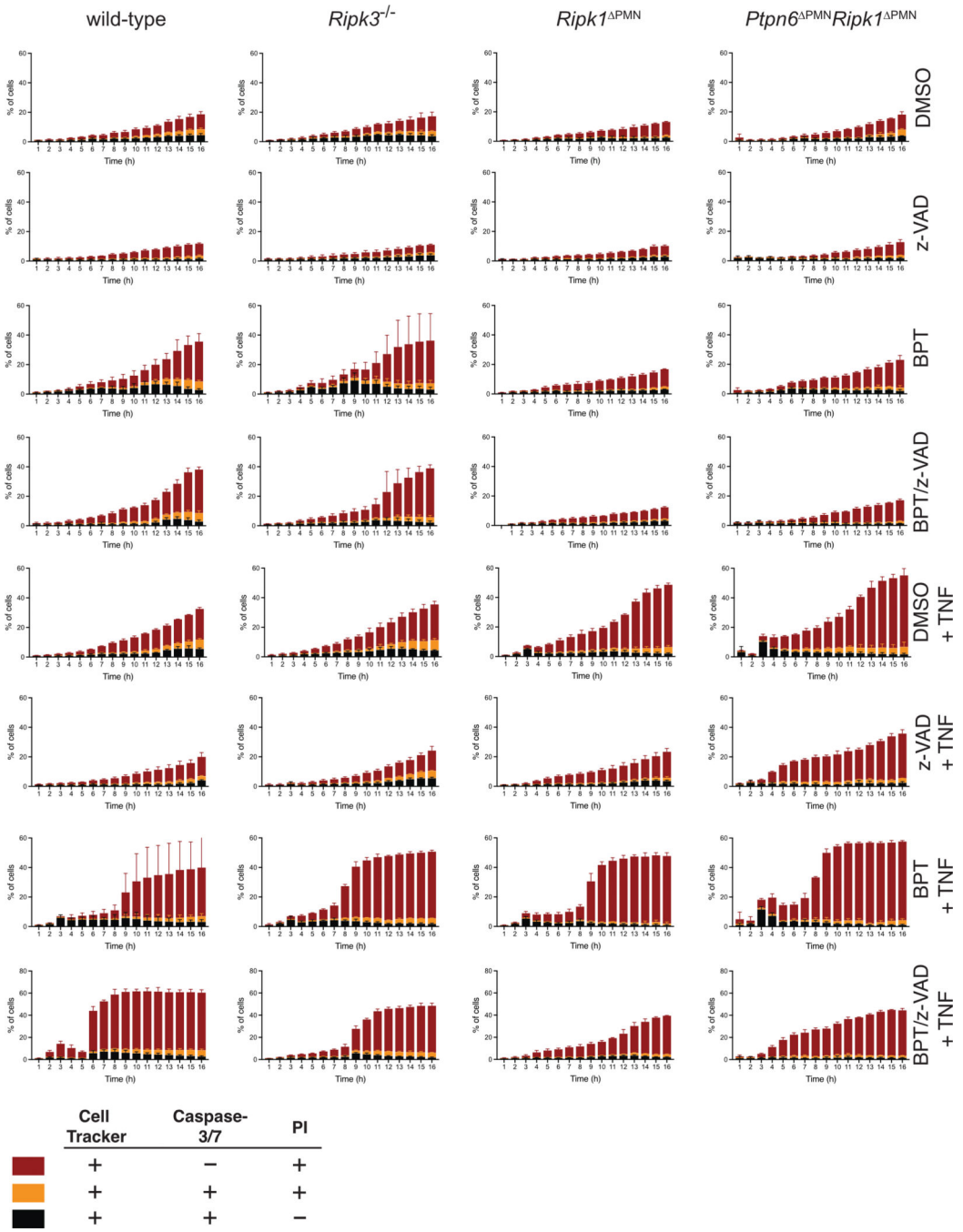

Extended Data 4. TNF induces caspase activation in the absence of Ripk1 in neutrophils.

Live-cell imaging of CellTracker Orange-labeled wild-type, *Ripk3*$^{-/-}$, *Ripk1*$^{\Delta PMN}$, and *Ptpn6*$^{\Delta PMN}$*Ripk1*$^{\Delta PMN}$ neutrophils treated with 2 μM BPT and/or 10 μM z-VAD-fmk +/− 100 ng/mL TNFα. CellEvent caspase-3/7 Green Detection Reagent and Draq7 were used to monitor changes in caspase activation and viability. Mean and SEM, n=3 technical triplicate samples from triplicate fields of view.

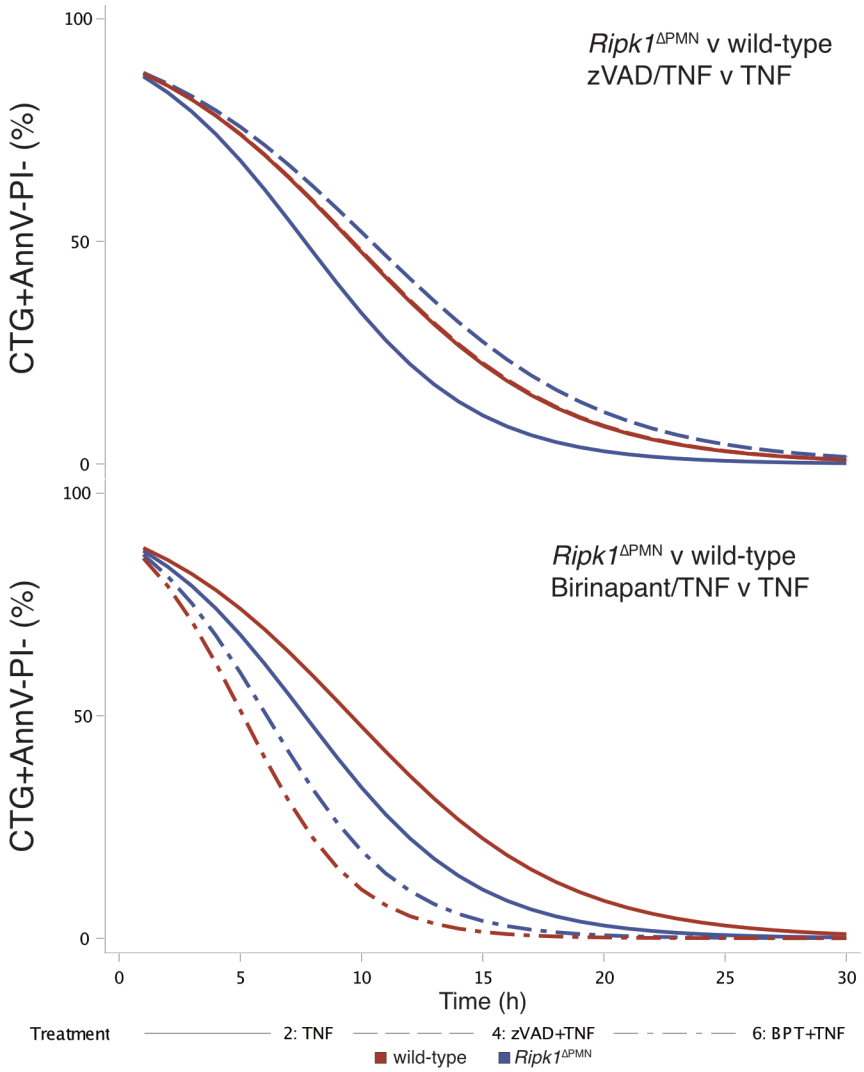

Extended Data 5. Generalized linear mixed effects models (logit link).

Comparison of CTG-positive proportion of **a)** z-VAD-fmk and **b)** birinapant treatment of TNF-stimulated *Ripk1*$^{\Delta PMN}$ and wild-type neutrophils. Red curves indicate predicted profiles for wild-type, blue for *Ripk1*$^{\Delta PMN}$, with line patterns indicating predicted profile for treatment.

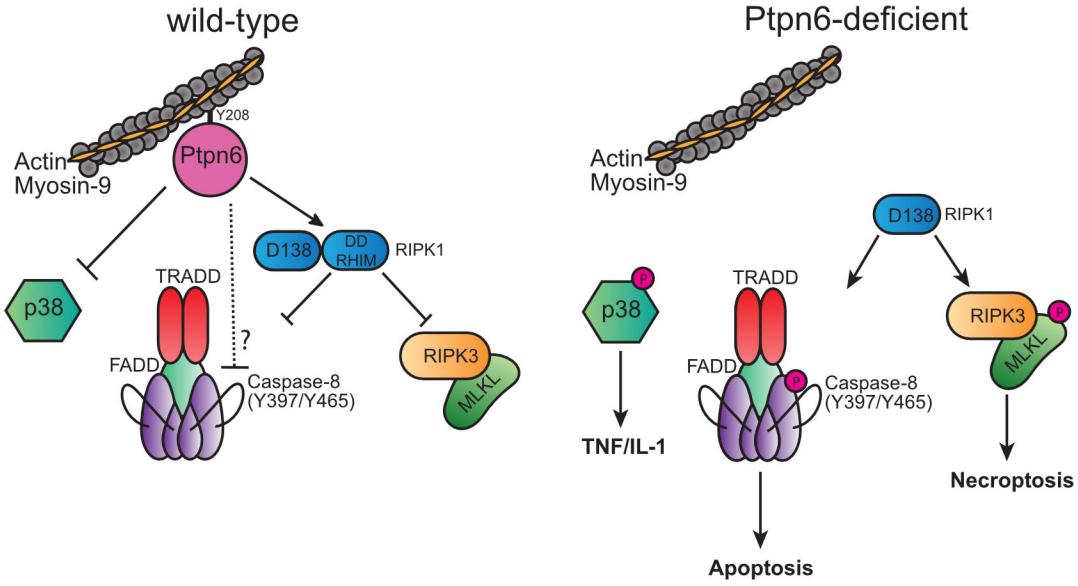

Extended Data 6. A model illustrating the role of Ptpn6 in regulation of cell death signaling in neutrophils.

Ptpn6 function is controlled in part by Y208-dependent anchoring to the actin-myosin-9 cytoskeleton. In the absence of Ptpn6, the negative regulatory functions of Ripk1 are lost but the kinase domain remains active to influence apoptotic and necroptotic cell death. In *Ptpn6*$^{\Delta PMN}$ neutrophils lacking RIPK1 kinase activity or RIPK1, necroptotic and apoptotic cell death proceed unabated.

Supplementary Material

Refer to Web version on PubMed Central for supplementary material.

Acknowledgements

Mlkl$^{-/-}$ mice were provided by W. S. Alexander (The Walter and Eliza Hall Institute of Medical Research). *Ripk3*$^{-/-}$ mice were provided by V. Dixit (Genentech). *Ripk1*$^{-/-}$, conditional *Ripk1*$^{fl/fl}$, and *Ripk1*^{D138N} mice were provided by M. Kelliher and M. Pasparakis, supported by NIH/AID Grant RO1 AI075118. Casp8 antibody was provided by A. Strasser (The Walter and Eliza Hall Institute of Medical Research). This work was supported by NIH Grant 5RO1HL124209 (BC), the American Asthma Foundation (BC), ISF grant #1416/15 and #818/18 (MG), alpha-1 foundation grant #615533 (MG, Recanati Foundation and the Varda and Boaz Dotan Research Center (MG), U.S.-Israel Binational Science Foundation (BSF) grant #2017176 (MG and BC), NHMRC Dora Lush Scholarship (JAO), and NHMRC Grants (637367, 1145788, 1162765). This work was supported by the Australian National Health and Medical Research Council (NHMRC) Independent Research Institutes Infrastructure Support Scheme grant (9000220), and a Victorian State Government Operational Infrastructure Support (OIS) grant, support from the Novo Nordisk Foundation provided to the Center for Biosustainability at the Technical University of Denmark (NNF10CC1016517: NEL), and NIGMS (R35 GM119850: IS). Live cell imaging performed at Boston Children's Hospital Intellectual Developmental Disabilities Research Center (IDDRC) is supported by grant 1U54HD0902565.

REFERENCES

1. Uihlein LC, Brandling-Bennett HA, Lio PA & Liang MG Sweet syndrome in children. Pediatr Dermatol 29, 38–44 (2012). [PubMed: 22011318]
2. Prat L, Bouaziz JD, Wallach D, Vignon-Pennamen MD & Bagot M Neutrophilic dermatoses as systemic diseases. Clin Dermatol 32, 376–388 (2014). [PubMed: 24767185]

3. Going JJ, Going SM, Myskow MW & Beveridge GW Sweet's syndrome: histological and immunohistochemical study of 15 cases. J Clin Pathol 40, 175–179 (1987). [PubMed: 3546396]

4. Bourke JF, Jones JL, Fletcher A & Graham-Brown RA An immunohistochemical study of the dermal infiltrate and epidermal staining for interleukin 1 in 12 cases of Sweet's syndrome. Br J Dermatol 134, 705–709 (1996). [PubMed: 8733376]

5. Giasuddin AS, El-Orfi AH, Ziu MM & El-Barnawi NY Sweet's syndrome: is the pathogenesis mediated by helper T cell type 1 cytokines? J Am Acad Dermatol 39, 940–943 (1998). [PubMed: 9843005]

6. Kluger N, Gil-Bistes D, Guillot B & Bessis D Efficacy of anti-interleukin-1 receptor antagonist anakinra (Kineret(R)) in a case of refractory Sweet's syndrome. Dermatology 222, 123–127 (2011). [PubMed: 21464561]

7. Beynon C et al. Successful Treatment of Autoimmune Disease-Associated Pyoderma Gangrenosum With the IL-1 Receptor Antagonist Anakinra: A Case Series of 3 Patients. J Clin Rheumatol 23, 181–183 (2017). [PubMed: 28333874]

8. Leuenberger M et al. PASS Syndrome: An IL-1-Driven Autoinflammatory Disease. Dermatology 232, 254–258 (2016). [PubMed: 26919742]

9. Acquitter M, Plantin P, Kupfer I, Auvinet H & Marhadour T Anakinra Improves Pyoderma Gangrenosum in Psoriatic Arthritis: A Case Report. Ann Intern Med 163, 70–71 (2015).

10. Nesterovitch AB et al. Alteration in the gene encoding protein tyrosine phosphatase nonreceptor type 6 (PTPN6/SHP1) may contribute to neutrophilic dermatoses. Am J Pathol 178, 1434–1441 (2011). [PubMed: 21406173]

11. Croker BA et al. Inflammation and autoimmunity caused by a SHP1 mutation depend on IL-1, MyD88, and a microbial trigger. Proc Natl Acad Sci U S A 105, 15028–15033 (2008). [PubMed: 18806225]

12. Croker BA et al. Neutrophils require SHP1 to regulate IL-1beta production and prevent inflammatory skin disease. J Immunol 186, 1131–1139 (2011). [PubMed: 21160041]

13. Abram CL, Roberge GL, Pao LI, Neel BG & Lowell CA Distinct roles for neutrophils and dendritic cells in inflammation and autoimmunity in motheaten mice. Immunity 38, 489–501 (2013). [PubMed: 23521885]

14. Shultz LD & Green MC Motheaten, an immunodeficient mutant of the mouse. II. Depressed immune competence and elevated serum immunoglobulins. J Immunol 116, 936–943 (1976). [PubMed: 56406]

15. Watson HA et al. Purity of transferred CD8(+) T cells is crucial for safety and efficacy of combinatorial tumor immunotherapy in the absence of SHP-1. Immunol Cell Biol 94, 802–808 (2016). [PubMed: 27430370]

16. Gurung P et al. Tyrosine Kinase SYK Licenses MyD88 Adaptor Protein to Instigate IL-1alpha-Mediated Inflammatory Disease. Immunity 46, 635–648 (2017). [PubMed: 28410990]

17. Thrall RS, Vogel SN, Evans R & Shultz LD Role of tumor necrosis factor-alpha in the spontaneous development of pulmonary fibrosis in viable motheaten mutant mice. Am J Pathol 151, 1303–1310 (1997). [PubMed: 9358756]

18. Bossaller L et al. Cutting edge: FAS (CD95) mediates noncanonical IL-1beta and IL-18 maturation via caspase-8 in an RIP3-independent manner. J Immunol 189, 5508–5512 (2012). [PubMed: 23144495]

19. Rickard JA et al. RIPK1 regulates RIPK3-MLKL-driven systemic inflammation and emergency hematopoiesis. Cell 157, 1175–1188 (2014). [PubMed: 24813849]

20. Wicki S et al. Loss of XIAP facilitates switch to TNFalpha-induced necroptosis in mouse neutrophils. Cell Death Dis 7, e2422 (2016). [PubMed: 27735938]

21. Miwa K et al. Caspase 1-independent IL-1beta release and inflammation induced by the apoptosis inducer Fas ligand. Nat Med 4, 1287–1292 (1998). [PubMed: 9809553]

22. Dillon CP et al. RIPK1 blocks early postnatal lethality mediated by caspase-8 and RIPK3. Cell 157, 1189–1202 (2014). [PubMed: 24813850]

23. Kaiser WJ et al. RIP1 suppresses innate immune necrotic as well as apoptotic cell death during mammalian parturition. Proc Natl Acad Sci U S A 111, 7753–7758 (2014). [PubMed: 24821786]

24. Oberst A et al. Catalytic activity of the caspase-8-FLIP(L) complex inhibits RIPK3-dependent necrosis. Nature 471, 363–367 (2011). [PubMed: 21368763]
25. Kaiser WJ et al. RIP3 mediates the embryonic lethality of caspase-8-deficient mice. Nature 471, 368–372 (2011). [PubMed: 21368762]
26. Alvarez-Diaz S et al. The Pseudokinase MLKL and the Kinase RIPK3 Have Distinct Roles in Autoimmune Disease Caused by Loss of Death-Receptor-Induced Apoptosis. Immunity 45, 513–526 (2016). [PubMed: 27523270]
27. Lukens JR et al. RIP1-driven autoinflammation targets IL-1alpha independently of inflammasomes and RIP3. Nature 498, 224–227 (2013). [PubMed: 23708968]
28. Roderick JE et al. Hematopoietic RIPK1 deficiency results in bone marrow failure caused by apoptosis and RIPK3-mediated necroptosis. Proc Natl Acad Sci U S A 111, 14436–14441 (2014). [PubMed: 25246544]
29. Zargarian S et al. Phosphatidylserine externalization, 'necroptotic bodies' release, and phagocytosis during necroptosis. PLoS Biol 15, e2002711 (2017). [PubMed: 28650960]
30. Gong YN et al. ESCRT-III Acts Downstream of MLKL to Regulate Necroptotic Cell Death and Its Consequences. Cell 169, 286–300 e16 (2017). [PubMed: 28388412]
31. Greten FR et al. NF-kappaB is a negative regulator of IL-1beta secretion as revealed by genetic and pharmacological inhibition of IKKbeta. Cell 130, 918–931 (2007). [PubMed: 17803913]
32. Kaiser WJ et al. Toll-like Receptor 3-mediated necrosis via TRIF, RIP3 and MLKL. J Biol Chem 288, 31268–31279 (2013). [PubMed: 24019532]
33. D'Cruz AA et al. The pseudokinase MLKL activates PAD4-dependent NET formation in necroptotic neutrophils. Sci Signal 11, eaao1716 (2018). [PubMed: 30181240]
34. Lalaoui N et al. Targeting p38 or MK2 Enhances the Anti-Leukemic Activity of Smac-Mimetics. Cancer Cell 29, 145–158 (2016). [PubMed: 26859455]
35. Jaco I et al. MK2 Phosphorylates RIPK1 to Prevent TNF-Induced Cell Death. Mol. Cell 66, 698–710 (2017). [PubMed: 28506461]
36. Dondelinger Y et al. MK2 phosphorylation of RIPK1 regulates TNF-mediated cell death. Nat. Cell Biol. 19, 1237–1247 (2017). [PubMed: 28920952]
37. Menon MB et al. P38 MAPK /MK2-dependent phosphorylation controls cytotoxic RIPK1 signalling in inflammation and infection. Nat. Cell Biol. 19, 1248–1259 (2017). [PubMed: 28920954]
38. Tartey S, Gurung P, Dasari TK, Burton A & Kanneganti TD ASK1/2 signaling promotes inflammation in a mouse model of neutrophilic dermatosis. J. Clin. Invest. 128, 2042–2047 (2018). [PubMed: 29629899]
39. de Graaf CA et al. Haemopedia: An Expression Atlas of Murine Hematopoietic Cells. Stem Cell Reports 7, 571–582 (2016). [PubMed: 27499199]
40. Mandal P et al. RIP3 induces apoptosis independent of pronecrotic kinase activity. Mol Cell 56, 481–495 (2014). [PubMed: 25459880]
41. Cook WD et al. RIPK1- and RIPK3-induced cell death mode is determined by target availability. Cell Death Differ 21, 1600–1612 (2014). [PubMed: 24902899]
42. Lawlor KE et al. XIAP Loss Triggers RIPK3- and Caspase-8-Driven IL-1beta Activation and Cell Death as a Consequence of TLR-MyD88-Induced cIAP1-TRAF2 Degradation. Cell Rep 20, 668–682 (2017). [PubMed: 28723569]
43. Yang Y, Fang S, Jensen JP, Weissman AM & Ashwell JD Ubiquitin protein ligase activity of IAPs and their degradation in proteasomes in response to apoptotic stimuli. Science (80-.). 288, 874–877 (2000).
44. Jia SH, Parodo J, Kapus A, Rotstein OD & Marshall JC Dynamic regulation of neutrophil survival through tyrosine phosphorylation or dephosphorylation of caspase-8. J Biol Chem 283, 5402–5413 (2008). [PubMed: 18086677]
45. Anderton H et al. RIPK1 prevents TRADD-driven, but TNFR1 independent, apoptosis during development. Cell Death Differ. 26, 877–889 (2019). [PubMed: 30185824]

46. Dowling JP, Alsabbagh M, Del Casale C, Liu ZG & Zhang J TRADD regulates perinatal development and adulthood survival in mice lacking RIPK1 and RIPK3. Nat. Commun. 10, 705 (2019). [PubMed: 30741936]
47. Newton K et al. RIPK1 inhibits ZBP1-driven necroptosis during development. Nature 540, 129–133 (2016). [PubMed: 27819682]
48. Moulin M et al. IAPs limit activation of RIP kinases by TNF receptor 1 during development. EMBO J 31, 1679–1691 (2012). [PubMed: 22327219]
49. Zhang J et al. Ubiquitin Ligases cIAP1 and cIAP2 Limit Cell Death to Prevent Inflammation. Cell Rep. 27, 2679–2689 (2019). [PubMed: 31141691]
50. Matalon O et al. Actin retrograde flow controls natural killer cell response by regulating the conformation state of SHP-1. EMBO J 37, e96264 (2018). [PubMed: 29449322]

METHODS-ONLY REFERENCES

51. Pao LI et al. B cell-specific deletion of protein-tyrosine phosphatase Shp1 promotes B-1a cell development and causes systemic autoimmunity. Immunity 27, 35–48 (2007). [PubMed: 17600736]
52. Shultz LD, Coman DR, Bailey CL, Beamer WG & Sidman CL 'Viable motheaten,' a new allele at the motheaten locus. I. Pathology. Am J Pathol 116, 179–192 (1984). [PubMed: 6380298]
53. Kelliher MA et al. The death domain kinase RIP mediates the TNF-induced NF-kappaB signal. Immunity 8, 297–303 (1998). [PubMed: 9529147]
54. Dannappel M et al. RIPK1 maintains epithelial homeostasis by inhibiting apoptosis and necroptosis. Nature 513, 90–94 (2014). [PubMed: 25132550]
55. Polykratis A et al. Cutting edge: RIPK1 Kinase inactive mice are viable and protected from TNF-induced necroptosis in vivo. J Immunol 193, 1539–1543 (2014). [PubMed: 25015821]
56. Newton K, Sun X & Dixit VM Kinase RIP3 is dispensable for normal NF-kappa Bs, signaling by the B-cell and T-cell receptors, tumor necrosis factor receptor 1, and Toll-like receptors 2 and 4. Mol Cell Biol 24, 1464–1469 (2004). [PubMed: 14749364]
57. Salmena L et al. Essential role for caspase 8 in T-cell homeostasis and T-cell-mediated immunity. Genes Dev 17, 883–895 (2003). [PubMed: 12654726]
58. Murphy JM et al. The pseudokinase MLKL mediates necroptosis via a molecular switch mechanism. Immunity 39, 443–453 (2013). [PubMed: 24012422]
59. Schindelin J et al. Fiji: an open-source platform for biological-image analysis. Nat Methods 9, 676–682 (2012). [PubMed: 22743772]
60. Andrews S FastQC - A quality control tool for high throughput sequence data. Babraham Bioinformatics http://www.bioinformatics.babraham.ac.uk/projects/ (2010). doi:citeulike-article-id:11583827
61. Patro R, Duggal G, Love MI, Irizarry RA & Kingsford C Salmon provides fast and bias-aware quantification of transcript expression. Nat. Methods 14, 417 (2017). [PubMed: 28263959]
62. Love MI, Huber W & Anders S Moderated estimation of fold change and dispersion for RNA-seq data with DESeq2. Genome Biol. 15, 550 (2014). [PubMed: 25516281]
63. Newman AM et al. Robust enumeration of cell subsets from tissue expression profiles. Nat. Methods 12, 453 (2015). [PubMed: 25822800]
64. Pedregosa F et al. Scikit-learn: Machine Learning in Python Gaël Varoquaux. J. Mach. Learn. Res. 12, 2825–2830 (2011).
65. Subramanian A et al. Gene set enrichment analysis: A knowledge-based approach for interpreting genome-wide expression profiles. Proc. Natl. Acad. Sci. 102, 15545–15550 (2005). [PubMed: 16199517]

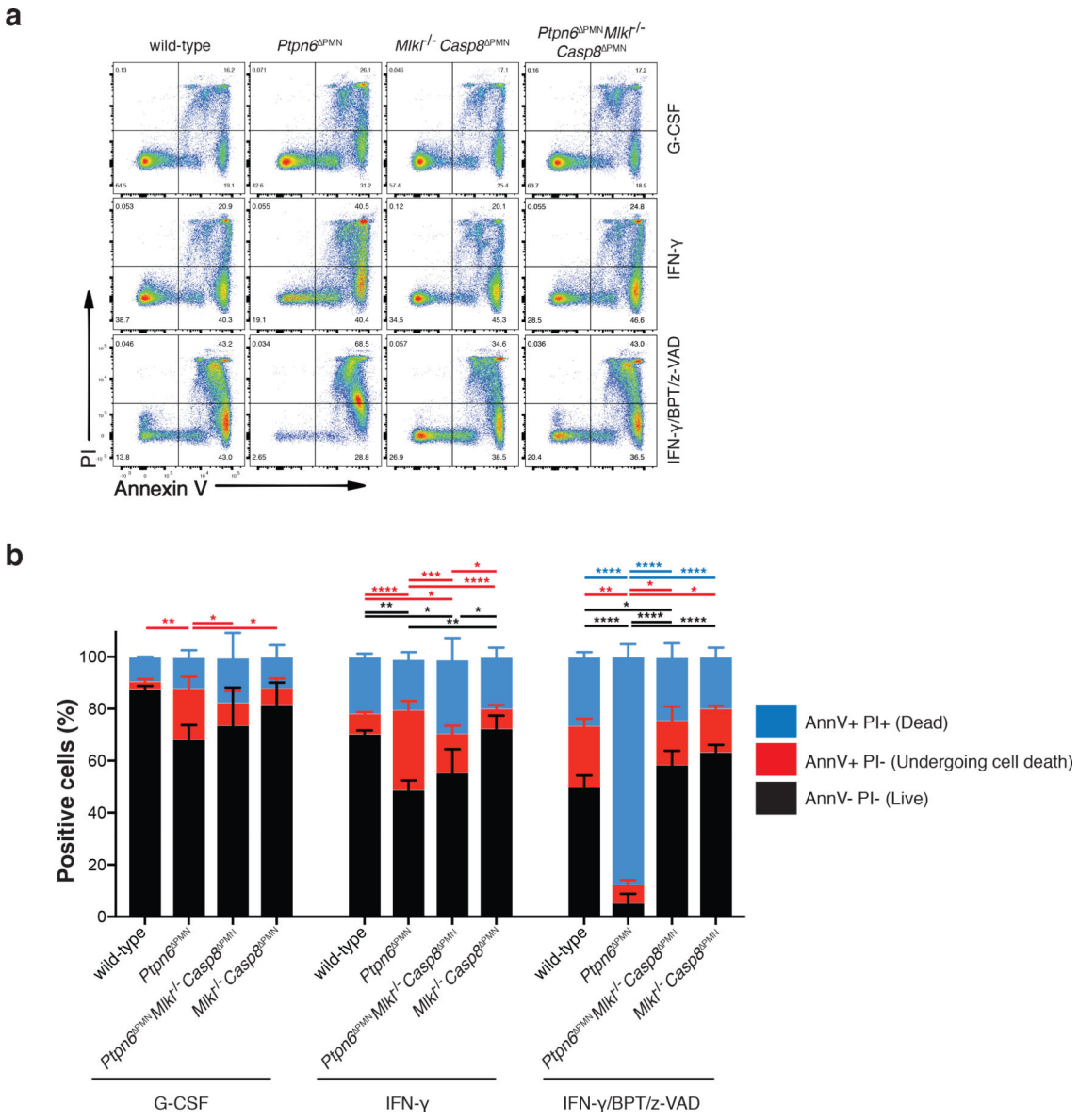

Figure 1. Loss of Ptpn6 sensitizes neutrophils to necroptotic cell death.

a-b) Flow cytometric analysis of wild-type, *Ptpn6*$^{\Delta PMN}$, *Caspase-8*$^{\Delta PMN}$*Mlkl*$^{-/-}$ and *Ptpn6*$^{\Delta PMN}$*Caspase-8*$^{\Delta PMN}$*Mlkl*$^{-/-}$ neutrophils stained with PI and Annexin V (Ann V) 12 h after addition of the necroptotic stimulus birinapant (BPT, 2 μM) + z-VAD-fmk (zVAD, 10 μM). Cells were first primed with 100 ng/mL G-CSF or 100 ng/mL IFN-γ. Mean ± SEM, n=3 biologically independent experiments. *p<0.05 ** p<0.01 ***p<0.001 ****p<0.0001, analyzed using one-way ANOVA with Tukey's multiple comparison test.

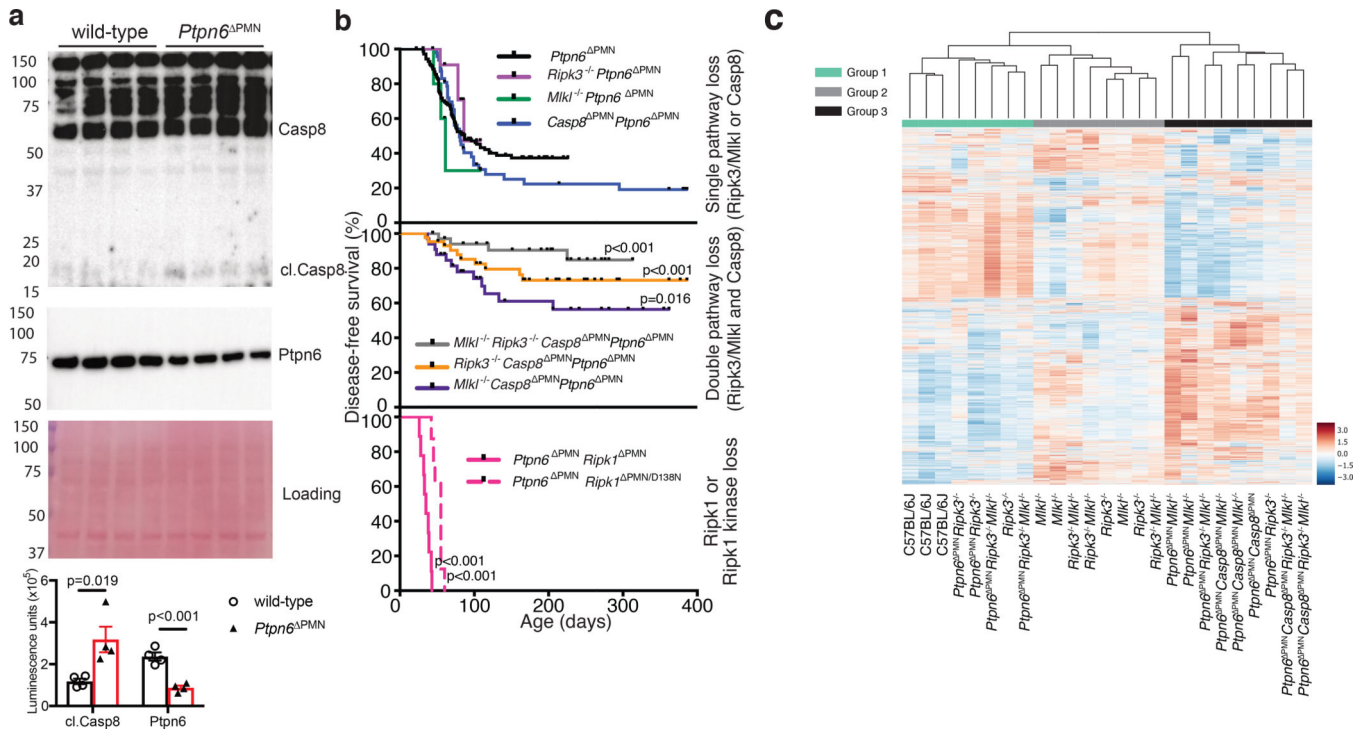

Figure 2. Caspase-8 and Ripk3/Mlkl drives footpad inflammation in *Ptpn6 mutant mice*

a) Immunoblot for cleaved caspase-8 and Ptpn6 from freshly-isolated wild-type and *Ptpn6*$^{\Delta PMN}$ bone marrow neutrophils. Luminescence was quantified using a ChemiDoc Gel Imaging System and ImageLab software. Mean ± SEM, n=4 independent neutrophil samples from *Ptpn6*$^{\Delta PMN}$ or wild-type littermate controls. Data analyzed by Student's t test. p values are shown. **b)** Kaplan-Meier plots showing disease-free survival of *Ptpn6*$^{\Delta PMN}$ mice (n=145) compared with *Ptpn6*$^{\Delta PMN}$*Ripk3*$^{-/-}$ (n=15), *Ptpn6*$^{\Delta PMN}$*Ripk3*$^{-/-}$*caspase-8*$^{\Delta PMN}$ (n=45) mice, *Ptpn6*$^{\Delta PMN}$*Mlkl*$^{-/-}$ (n=10), *Ptpn6*$^{\Delta PMN}$*caspase-8*$^{\Delta PMN}$*Mlkl*$^{-/-}$ (n=35) mice, *Ptpn6*$^{\Delta PMN}$*caspase-8*$^{\Delta PMN}$ (n=49), *Ptpn6*$^{\Delta PMN}$*caspase-8*$^{\Delta PMN}$*Ripk3*$^{-/-}$*Mlkl*$^{-/-}$ (n=34), *Ptpn6*$^{\Delta PMN}$*Ripk1*$^{\Delta PMN}$ (n=9) and *Ptpn6*$^{\Delta PMN}$*Ripk1*$^{\Delta PMN/D138N}$ (n=8) mice. Survival curves were analyzed using a log-rank (Mantel-Cox) test compared to *Ptpn6*$^{\Delta PMN}$ mice. Each panel shares the disease-free survival data of *Ptpn6*$^{\Delta PMN}$ mice. **c)** RNA-Seq transcriptomic analysis of bone marrow neutrophils from female *Ptpn6*$^{\Delta PMN}$ mice lacking *Ripk3*, *Mlkl*, and/or *Casp8*. Values are gene-wise z-scores of counts using the variance stabilized transformation from DESeq2.

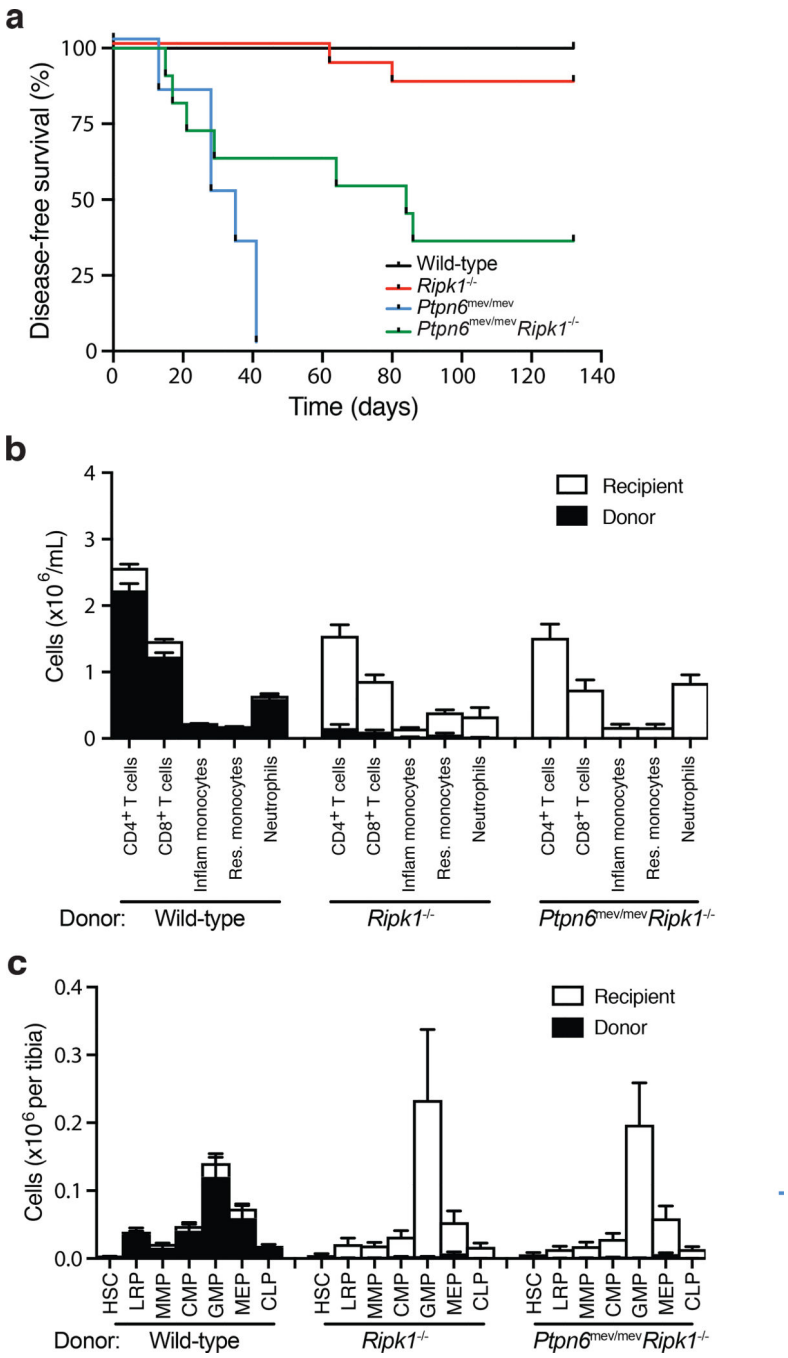

Figure 3. RIPK1-deficiency prevents lethal inflammatory disease in Ptpn6 mutant mice by impairing hematopoiesis.

a) Kaplan-Meier plot comparing disease-free survival of lethally-irradiated wild-type mice transplanted with 10^6 *Ripk1*$^{-/-}$, *Ptpn6*$^{mev/mev}$*Ripk1*$^{-/-}$, *Ptpn6*$^{mev/mev}$ or wild-type fetal liver cells. Survival curves were analyzed using a log-rank (Mantel-Cox) test. p<0.0001, wild-type v *Ptpn6*$^{mev/mev}$; p=0.0025, wild-type v *Ptpn6*$^{mev/mev}$*Ripk1*$^{-/-}$; p=0.0454, *Ptpn6*$^{mev/mev}$ v *Ptpn6*$^{mev/mev}$*Ripk1*$^{-/-}$; p<0.0001, *Ptpn6*$^{mev/mev}$ v *Ptpn6*$^{mev/mev}$*Ripk1*$^{-/-}$. **b-c)** Characterization of the **(b)** hematopoietic compartment in peripheral blood 12 weeks post-

transplant and **(c)** progenitor cells in the bone marrow of recipient mice 20 weeks post-transplant with 10^6 wild-type, *Ripk1*$^{-/-}$ or *Ptpn6*$^{mev/mev}$*Ripk1*$^{-/-}$ fetal liver cells. In **(c)**, counts of hematopoietic stem cells (HSC), lineage-restricted progenitors (LRP), multipotent progenitors (MPP), common myeloid progenitors (CMP), granulocyte-macrophage progenitors (GMP), megakaryocyte-erythroid progenitors (MEP), and common lymphoid progenitors (CLP) from the bone marrow of lethally-irradiated recipients 20 weeks post-transplant, mean ± SEM, n = 4. $p<0.05$ for all comparisons of *Ptpn6*$^{mev/mev}$*Ripk1*$^{-/-}$ and *Ripk1*$^{-/-}$ to wild-type.

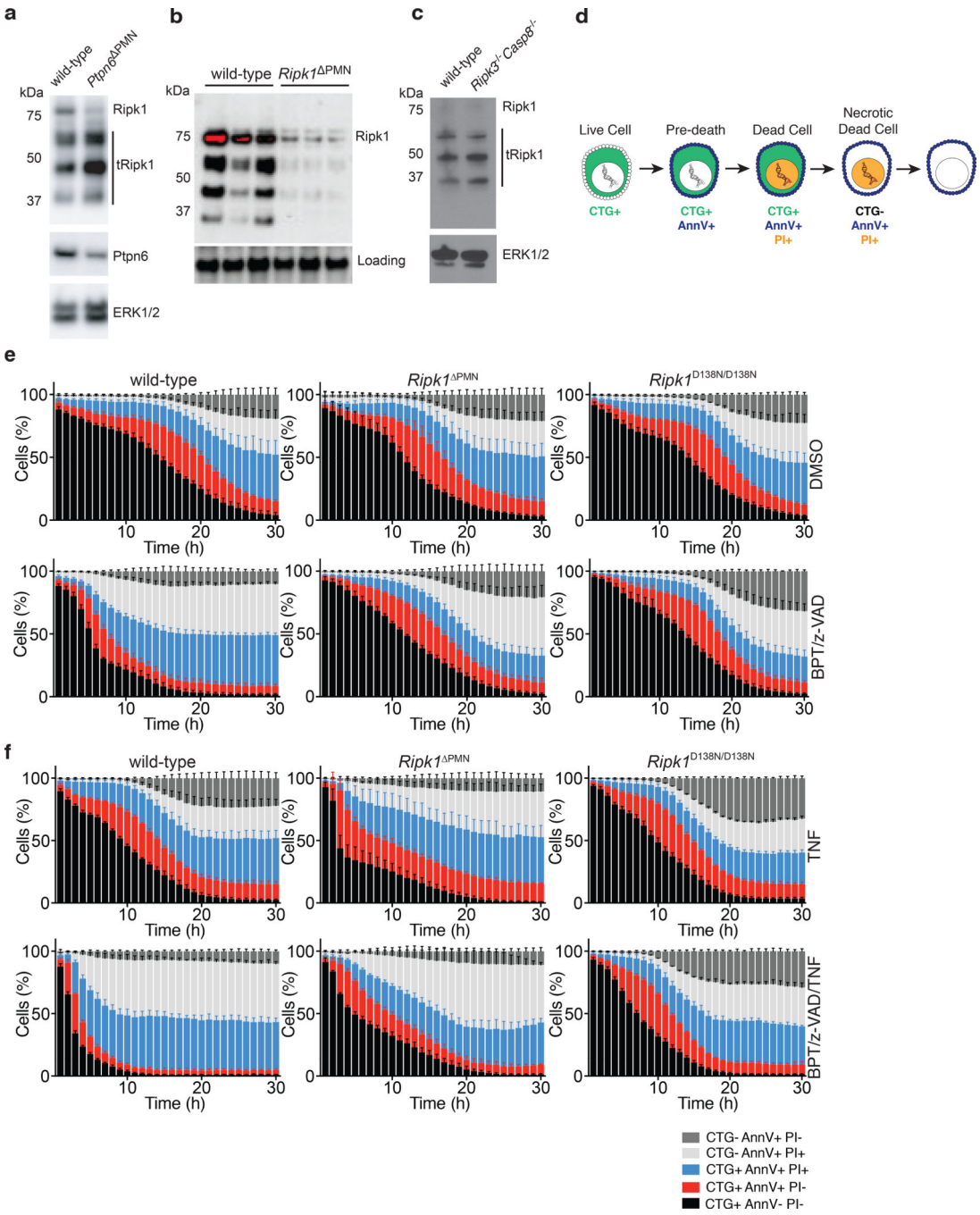

Figure 4. Loss of RIPK1 sensitizes neutrophils to TNF-mediated cell death.

a) Immunoblot showing Ripk1 and Ptpn6 in peripheral blood neutrophils isolated from wild-type and *Ptpn6*$^{\Delta PMN}$ mice. ERK p42/44 is a loading control. Neutrophils pooled from 10–11 independent mice. Representative of 3 biologically independent experiments. **b)** Immunoblot for Ripk1 in lysates of bone marrow neutrophils from three independent *Ripk1*$^{\Delta PMN}$ mice. **c)** Immunoblot for full-length and truncated Ripk1 (tRipk1) in lysates of wild-type and *Ripk3*$^{-/-}$*Casp8*$^{-/-}$ bone marrow neutrophils. Representative data of 2 biologically independent experiments. **d)** Cell transition states identified by live cell imaging during

regulated cell death of neutrophils. **e-f)** Live-cell imaging of CTG-labeled wild-type, *Ripk1*$^{\Delta PMN}$, and *Ripk1*$^{D138N/D138N}$ neutrophils treated with DMSO (e, top row), BPT/z-VAD (e, bottom row), TNF (f, top row), or BPT/z-VAD/TNF (f, bottom row) (drug concentrations: 2 μM BPT, 10 μM z-VAD-fmk, 100 ng/mL TNF). PI and Annexin V were used to monitor changes in viability. Mean and SEM, n=3 biologically independent experiments, and triplicate fields of view per biological replicate. BPT: birinapant; z-VAD: z-VAD-fmk; CTG: Cell Tracker Green; PI: propidium iodide.

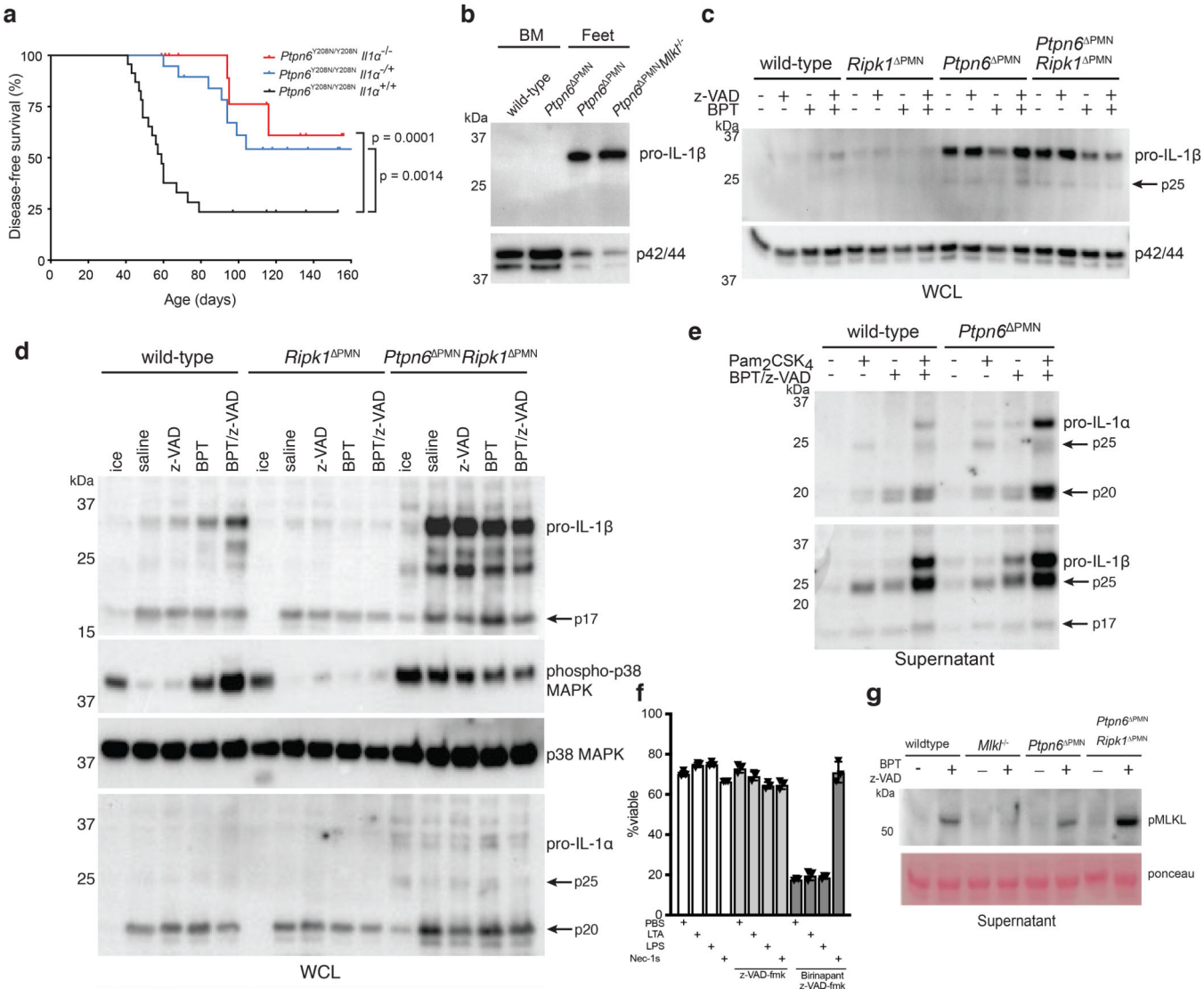

Figure 5. Ptpn6-deficient neutrophils produce high levels of IL-1α and IL-1β in the absence of Ripk1.

a) Kaplan-Meier plot comparing disease-free survival of *Ptpn6*$^{Y208N/Y208N}$*Il1a*$^{+/+}$ (n=23) mutant mice with *Ptpn6*$^{Y208N/Y208N}$*Il1a*$^{-/-}$ (n=23) and *Ptpn6*$^{Y208N/Y208N}$*Il1a*$^{+/-}$ (n=19) mice. Survival curves were analyzed using a log-rank (Mantel-Cox) test compared to *Ptpn6*$^{\Delta PMN}$*Il1a*$^{+/+}$ mice. p values are indicated. **b)** Immunoblot of IL-1β in neutrophils isolated from the bone marrow of wild-type and *Ptpn6*$^{\Delta PMN}$ mice, or neutrophils pooled from the feet of three inflamed *Ptpn6*$^{\Delta PMN}$ and two inflamed *Ptpn6*$^{\Delta PMN}$*Mlkl*$^{-/-}$ mice. Representative of 3 biologically independent experiments. **c)** Immunoblot for IL-1β from whole cell lysates of wild-type, *Ptpn6*$^{\Delta PMN}$, *Ripk1*$^{\Delta PMN}$, and *Ptpn6*$^{\Delta PMN}$ *Ripk1*$^{\Delta PMN}$ bone marrow neutrophils primed for 1h with 100ng/mL IFNγ, and treated for 4 h with 2 μM BPT and/or 10 μM z-VAD-fmk, Representative of 3 biologically independent experiments. **d)** Immunoblot for IL-1β, IL-1α, p38 MAPK, and phospho-p38 MAPK from whole cell lysates of wild-type, *Ripk1*$^{\Delta PMN}$, and *Ptpn6*$^{\Delta PMN}$ *Ripk1*$^{\Delta PMN}$ neutrophils primed for 1h with 100ng/mL IFNγ, and treated for 4 h with 2 μM BPT and/or 10 μM z-VAD-fmk.

Representative of 3 biologically independent experiments. ERK p42/44 was used as a loading control. **e)** Western blot showing IL-1α and IL-1β in the supernatant of wild-type and *Ptpn6*$^{\Delta PMN}$ neutrophils treated overnight with the necroptotic stimuli BPT (2 μM) + z-VAD-fmk (10 μM) and/or 10 ng/mL Pam_2CSK_4, Representative of 3–4 independent experiments. **f)** Bone marrow neutrophil viability measured by PI uptake of neutrophils treated with 1 μg/mL lipotechoic acid, 100 ng/mL LPS or 10 μM Nec-1s in the presence of 10 μM z-VAD-fmk +/− 2 μM BPT. Mean ± SEM, n = 3 independent samples. LPS: lipopolysaccharide; LTA: lipoteichoic acid; Nec-1s: necrostatin-1s. **g)** Immunoblot for phospho-Mlkl in supernatant of neutrophils treated with BPT/z-VAD overnight. Ponceau staining is used as a loading control. Representative of 3 independent experiments.

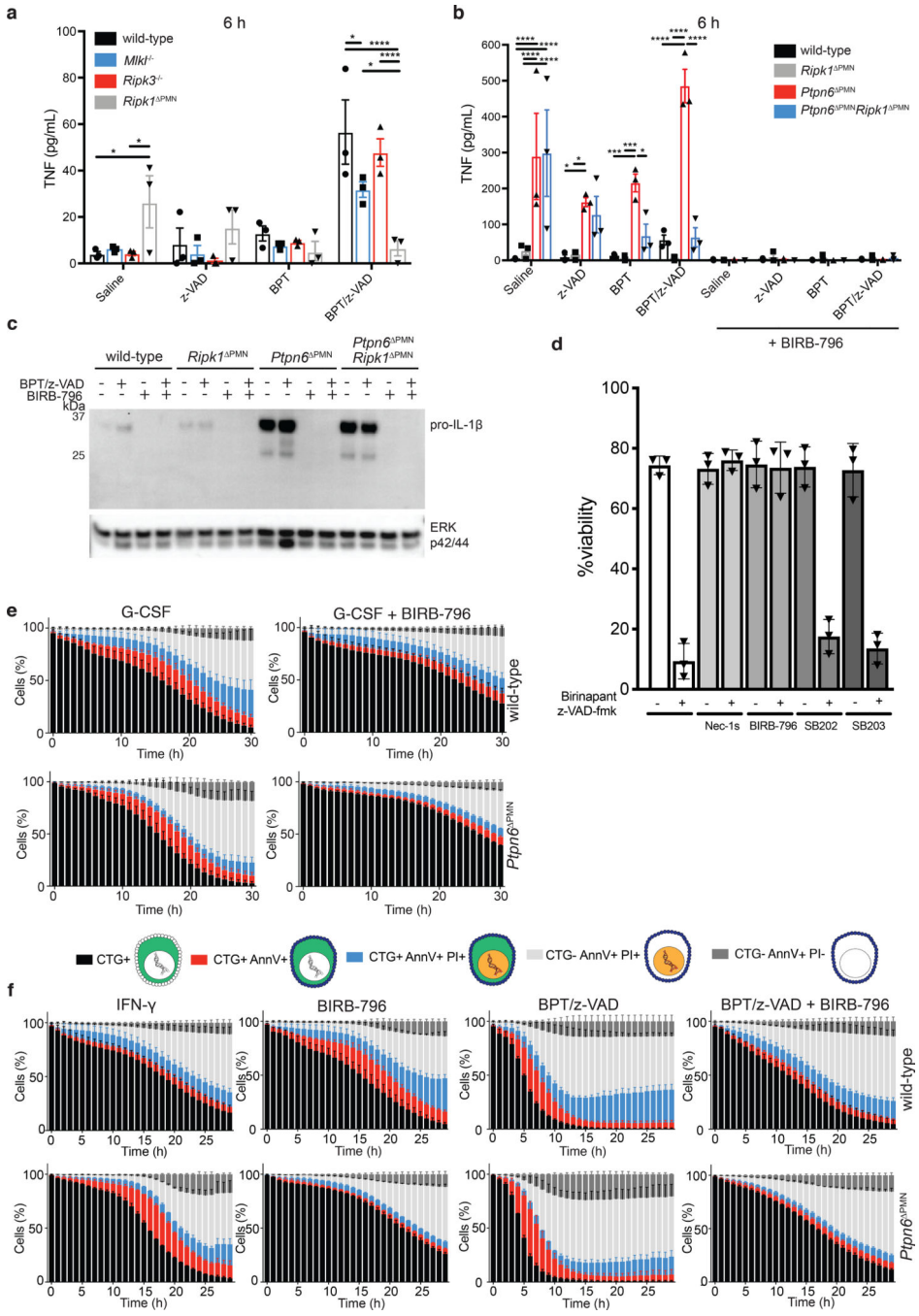

Figure 6. p38 signaling drives TNF and IL-1 production by Ptpn6-deficient neutrophils in the absence of Ripk1.

a-b) Wild-type, *Mlkl*$^{-/-}$, *Ripk3*$^{-/-}$, *Ripk1*$^{\Delta PMN}$, *Ptpn6*$^{\Delta PMN}$, and *Ptpn6*$^{\Delta PMN}$*Ripk1*$^{\Delta PMN}$ neutrophils were primed for 1 h with 100 ng/mL IFN-γ before addition of 2 μM BPT and/or 10 μM z-VAD-fmk +/− 20 μM BIRB-796. TNF-α in the supernatant was measured after 6 h by ELISA. Mean and SEM, n=3 biologically independent experiments *p<0.05, **p<0.01, ***p<0.001, ****p<0.0001, analyzed using one-way ANOVA with Tukey's multiple comparison test. **c)** Immunoblot of IL-1β in whole cell lysates after 4 h incubation. ERK

p42/44 was used as a loading control. n = 3 biologically independent experiments. BPT: birinapant; z-VAD: z-VAD-fmk. **d)** Bone marrow neutrophils were treated with 2 μM birinapant and 10 μM z-VAD-fmk for 15h in the presence or absence of necrostatin-1s (Nec-1s), or the p38 inhibitors SB202190, SB203580 and BIRB-796. Viability was assessed by flow cytometry using propidium iodide (PI). Mean and SEM, n=3 biologically independent experiments. **e-f)** Live-cell imaging of CellTracker Green (CTG)-labeled wild-type and *Ptpn6*$^{\Delta PMN}$ neutrophils treated with 100 ng/mL G-CSF, or 100 ng/mL IFN-γ, 2 μM birinapant, 10 μM z-VAD-fmk, +/− 20 μM BIRB-796. PI and Annexin V were used to monitor changes in viability. Mean and SEM, n=3 biologically independent experiments. BPT: birinapant; z-VAD: z-VAD-fmk

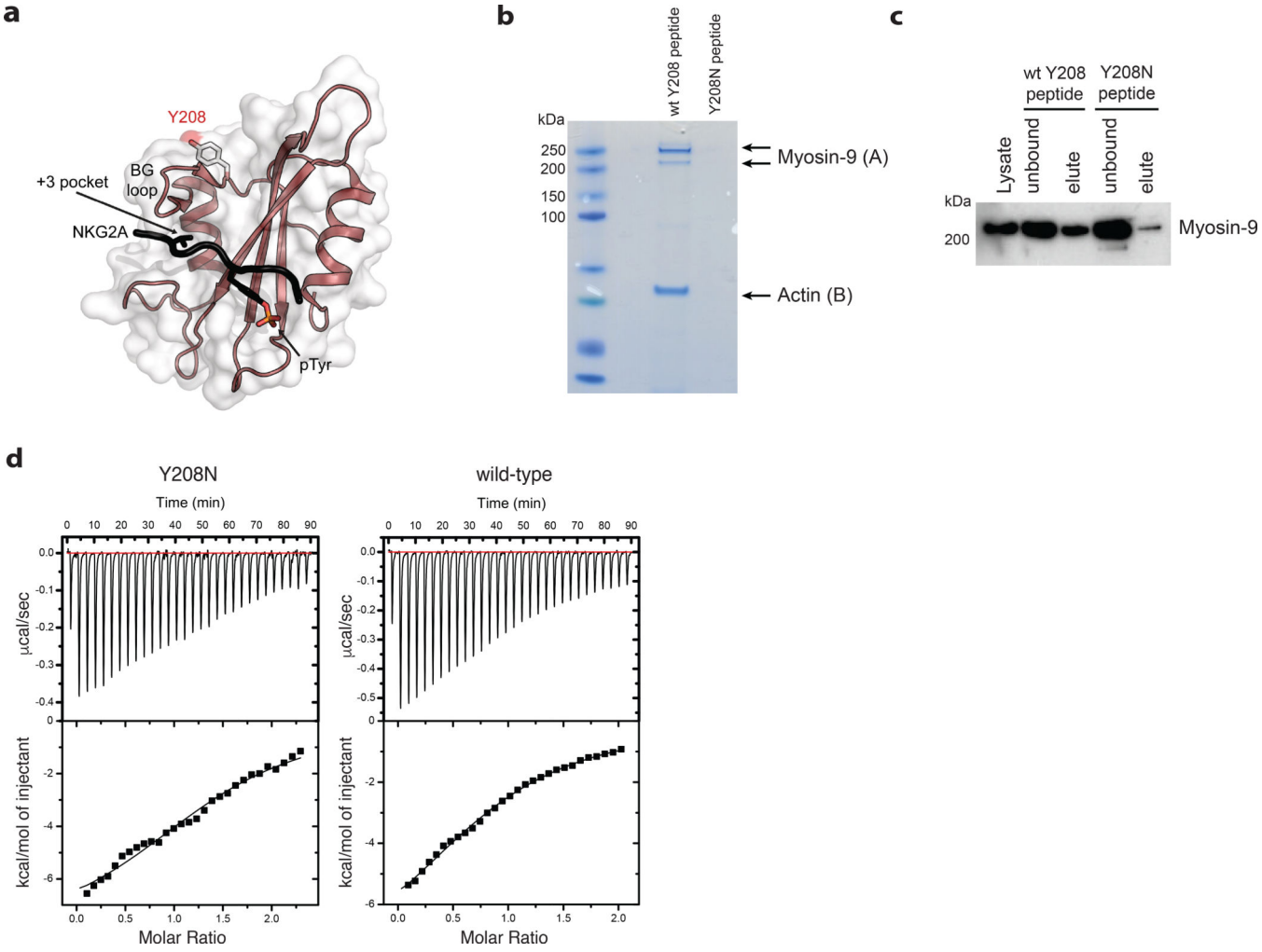

Figure 7. Ptpn6 contact with the actin-myosin cytoskeleton is mediated by Y208.

a) The structure of the Ptpn6 C-terminal SH2 domain bound to a phosphopeptide derived from the Natural Killer Group 2A (NKG2A) protein is displayed (PDB ID: 2YU7). The solvent accessible surface of the Ptpn6 SH2 domain (white) is shown overlaid on a ribbon diagram of the domain. The bound NKG2A phosphopeptide is shown in black with the phosphotyrosine residue indicated in stick representation. Tyrosine 208 is located at the C-terminal end of the BG loop. It is solvent accessible and does not contact the specificity-determining pocket (+3 pocket), nor the phosphotyrosine binding pocket. **b)** Coomassie staining for proteins associated with the wild-type and Y208N mutant Ptpn6 C-SH2 domains following immunoprecipitation from 10^8 neutrophils. Representative data from two biologically independent experiments. Peptides isolated from gel slices in (A) and (B) are described in Supplementary Table 2. **c)** Immunoblot for Myosin-9 in 5×10^6 neutrophils following immunoprecipitation with the biotinylated peptides corresponding to the wild-type and Y208N mutant Ptpn6 C-SH2 domain. Representative data from three biologically independent experiments. **d)** Isothermal titration calorimetry (ITC) analysis comparing the

interaction of FcγR2b phosphopeptide with wild-type and Y208N mutant recombinant C-terminal SH2 domain. Representative data from two biologically independent experiments.